IEEE Access
Multidisciplinary ⋮ Rapid Review ⋮ Open Access Journal

Received 14 August 2024, accepted 11 October 2024, date of publication 21 October 2024, date of current version 8 November 2024.

Digital Object Identifier 10.1109/ACCESS.2024.3483940

RESEARCH ARTICLE

Joint Subcarrier Time Reference Index-Modulation-Aided Differential Chaos Shift Keying Communication System

FADHIL S. HASAN[1] **AND ALEJANDRO A. VALENZUELA**[2]
[1]College of Engineering, Mustansiriyah University, Baghdad 14022, Iraq
[2]Department of Engineering and Communication, Bonn-Rhein-Sieg University of Applied Sciences, 53757 Sankt Augustin, Germany

Corresponding authors: Fadhil S. Hasan (fadel_sahib@uomustansiriyah.edu.iq) and Alejandro A. Valenzuela (alejandro.valenzuela@h-brs.de)

This work was supported in part by the College of Engineering of Mustansiriyah University, and in part by the German-Argentinean University Centre Deutsch-Argentinisches Hochschulzentrum (DAHZ)-Centro Universitario Argentino-Alemán (CUAA).

ABSTRACT A novel multidimensional index modulation-based differential chaos shift keying (DCSK) technique, designated as Joint Subcarrier Time Reference Index Modulation-aided Differential Chaos Shift Keying (JSTRIM-DCSK), is proposed for efficient data transmission in chaotic communication systems. The JSTRIM-DCSK system integrates subcarrier, time slot, and reference signal indexing to transmit information and offers two variants: JSTRIM-DCSK-I and JSTRIM-DCSK-II. The data is organized into L subblocks, each containing N_s subcarrier index bits p_s and N_t time slot index bits p_t, reference index bits p_r, and modulated bits p_m. The subcarrier and time slot index bits jointly select an active or inactive subcarrier time slot combination from a total of N_sN_t possibilities, categorizing the system as either JSTRIM-DCSK-I (active) or JSTRIM-DCSK-II (inactive). The reference indexed bits select a single chaotic reference signal from N_r orthogonal chaotic vectors generated using the Gram-Schmidt orthogonalization process. The modulated bits are transmitted using a DCSK modulation scheme. Analytical expressions for the bit error rate (BER) performance of the JSTRIM-DCSK system are derived under both additive white Gaussian noise (AWGN) and multipath Rayleigh fading channel (MRFC) conditions. Furthermore, the potential for energy savings, bandwidth efficiency, and system complexity of the JSTRIM-DCSK system are thoroughly analyzed and compared with those of the existing techniques. The simulation results validate the analytical expressions and demonstrate the potential of JSTRIM-DCSK to achieve high data rates, efficient energy savings, and a competitive BER performance.

INDEX TERMS Chaos communications, modulation coding, multidimensional coding, multipath channels, subcarrier multiplexing.

I. INTRODUCTION

The increasing demand for efficient and robust communication systems in high-data-rate applications motivates the development of innovative modulation techniques. Traditional methods frequently encounter difficulties in achieving an optimal balance between spectral efficiency, energy efficiency, and system complexity, particularly in environments with fluctuating channel conditions. Chaos-based modulation techniques address some of these challenges by employing easily generated wide-bandwidth chaotic signals. The differential chaos shift keying (DCSK) scheme, initially proposed in [1] as a means of addressing the challenges associated with receiver synchronization [2], represents a significant advancement in chaos-based communication systems. Its widespread adoption and extensive study in chaos spread spectrum systems can be attributed to its low-complexity implementation, independence from channel information at

The associate editor coordinating the review of this manuscript and approving it for publication was Qilian Liang.

the receiver, and commendable performance, particularly over selective Rayleigh fading channels [3]. Consequently, DCSK has attracted considerable attention and has been employed in a multitude of communication systems, including multiple-input multiple-output (MIMO) systems [4], underwater acoustic communication systems [5], power line communication systems [6], network coding systems [7], wireless power transfer systems [8], and free-space optical communication systems [9]. However, DCSK is not without limitations, particularly those associated with the transmission of reference chaotic signals in the initial time slot of the symbol period. This ultimately results in diminished data rates, reduced energy efficiency, and increased error rates. To address these limitations, extensive research has been conducted to enhance classical DCSK systems. These include quadrature chaos shift keying (QCSK) [10], high-efficiency DCSK (HE-DCSK) [11], code-shifted DCSK (CS-DCSK) [12], generalized CS-DCSK (GCS-DCSK) [13], high-data-rate CS-DCSK (HCS-DCSK) [14], a combination of M-ary constellations with DCSK [15], [16], [17], shortening of the reference signal [18] over orthogonal chaotic vector shift keying (OCVSK) [19], [20], [21], noise reduction DCSK (NR-DCSK) approaches [22], which involve repeating short chaotic signals multiple times, and the use of low-density parity check code (LDPC) [23], [24]. Furthermore, orthogonal frequency-division multiplexing (OFDM) has also been integrated with differential chaos shift keying (DCSK) to enhance information rate, bandwidth, and energy efficiency [25], [26], [27], [28], [29].

Recently, index modulation (IM) techniques have emerged to improve the data rate, bandwidth, and energy efficiency of traditional communication systems [30], [31]. The data rate in the IM system is enhanced without additional energy consumption and with a simple increase in complexity. It transmits data through the index of entities, such as frequency (subcarrier), time slot, code, spatial, or a hybrid between them. Further proposals include power coefficient optimization, as in code index modulation DCSK (CIM-DCSK) and CIM short reference DCSK (CIM-SR-DCSK) [32], [33], code index modulations integrated with generalized code-shift DCSK, multilevel code-shifted DCSK [34], [35], and the combination of carrier index (CI) modulation with DCSK [36], [37], [38]. Commutation CI DCSK (CCI-DCSK) introduces orthogonal commutation signals selected by mapping bits [39]. Permutation index CI DCSK (PI-DCSK) employs a single orthogonal permutation signal chosen by a mapping bit to transmit the modulated bit [40]. In [41], a dual index modulation DCSK (DCSK-DIM) using two parallel time slot indices has been proposed. Other improvements to DCSK include combining M-ary OCVSK with index modulation to form MC-MOCVSK-IM, using hybrid subcarrier and code indices in joint carrier-code index modulation aided M-ary differential chaos shift keying systems (JCCIM-MDCSK), and integrating grouping subcarrier index modulation into DCSK [42], [43], [44], [45], [46], [47], [48]. In [49], a neural network (NN) is utilized to improve the bit error rate (BER) performance of an index-modulated DCSK system. In a recent study, a joint carrier-time-code-sort index modulation DCSK (JCTCS-IM-DCSK) system has been proposed to improve the performance of high data rate DCSK systems [50].

Our work addresses these challenges by introducing the JSTRIM-DCSK system, a novel communication approach that integrates joint subcarrier time reference index modulation with DCSK. Unlike previous systems such as GSIM-DCSK [44], GSPIM-DCSK [48], and CTIM-DCSK [47], JSTRIM-DCSK enhances the characteristic analysis while maintaining the complexity per bit. It uses multidimensional index modulation based on subcarrier, time, and reference index resources to achieve high data rate and energy efficiency. In the proposed system, the Gram-Schmidt orthogonalization algorithms generate orthogonal chaotic reference signals, thereby improving spectral efficiency.

We derive analytical expressions for the bit error rate over AWGN and MRFC and confirm their accuracy through simulations. This validation demonstrates the robustness and effectiveness of our proposed systems under various channel conditions. Our work includes a detailed comparison of the proposed systems with recent advances, focusing on energy efficiency, bandwidth efficiency, and complexity, highlighting their competitive advantages and potential applications in various communication scenarios.

II. THE JSTRIM-DCSK SYSTEM

JSTRIM-DCSK introduces two schemes, JSTRIM-DCSK-I and JSTRIM-DCSK-II, which divide the information bits into L groups with specific bit allocations. Reference index bits select a reference chaotic signal, while subcarrier time index bits indicate the active or inactive Analytical expressions for the bit error rate (BER) are derived for both additive white Gaussian noise and multipath Rayleigh fading channels, with simulation results confirming the theory and comparing it with recent advances.

A. THE JSTRIM-DCSK-I SCHEME

The transmitter side block diagram of the proposed JSTRIM-DCSK-I system is shown in Fig. 1. The system involves a single modulated bit for each symbol. First, the Gram-Schmidt orthogonalization algorithm (GSA) is used to derive orthogonal chaotic signals from a set of N_r chaotic generators, each of length R. The chaotic generators use a second-order Chebyshev polynomial function $z_{q,k+1} = 1 - 2z_{q,k}^2$, where $k = 0, 1, \ldots, R$ and $q = 1, 2, \ldots, N_r$, with different initial values. These chaotic signals, proven to be uncorrelated and linearly independent [28], [42], are transformed by the GSA to perfectly normalized orthogonal signals, all with the same vector length. For $k = 1, .., R$ the N_r reference-chaotic signals, forming a matrix $X \in \mathbb{R}^{N_r \times R}$,

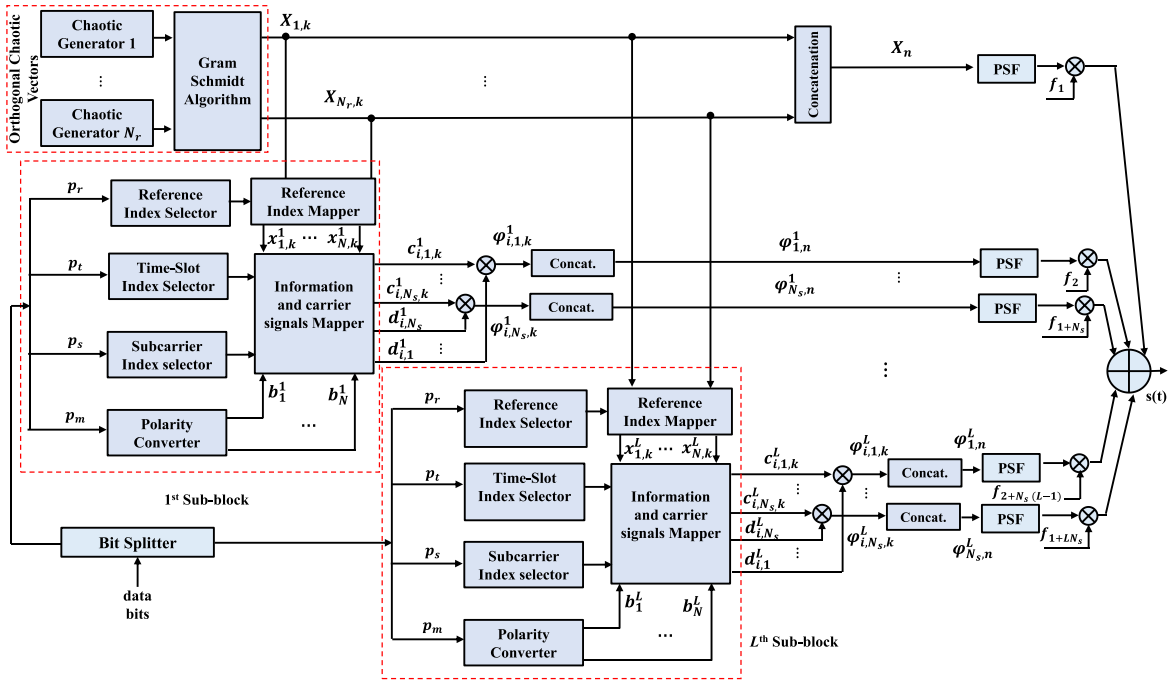

FIGURE 1. JSTRIM-DCSK transmitter.

is defined as

$$X_{q,k} = \begin{cases} \dfrac{z_{1,k}}{\sqrt{\sum_{k=1}^{R}\left[z_{1,k}\right]^2}}, \\ \qquad q = 1 \\ \dfrac{z_{q,k} - \sum_{m=1}^{n-1}\left[\sum_{k=1}^{R} z_{q,k}X_{m,k}\right]X_{m,k}}{\sqrt{\sum_{k=1}^{R}\left[z_{q,k} - \sum_{m=1}^{n-1}\left(\sum_{k=1}^{R} z_{q,k}X_{m,k}\right)X_{m,k}\right]^2}}, \\ \qquad q = 2, 3, .., N_r. \end{cases} \tag{1}$$

This expression defines the k^{th} sample of the q^{th} orthogonal chaotic signal: By concatenating these reference-chaotic signals, they are transformed into a unified vector X_n with a length of $\beta = N_r R$, where β is the spreading factor, $n = 1, \ldots, \beta$, $X_n = X_{k+(q-1)R} = X_{q,k}, q \in 1, \ldots, N_r$ and $k = 1, \ldots, R$. The JSTRIM-DCSK symbol is composed of L groups. Each group consists of $p_s + p_t + p_r + p_m$ bits, where p_s, p_t, p_r and p_m represent subcarrier, time, reference, and modulated bits, respectively. In the JSTRIM-DCSK-I, the number of modulated bits is equal to one. Consequently, the total number of transmitted bits amounts to a value of Lp_I bits, where $p_I = p_s + p_t + p_r + 1$. Each symbol group comprises the bits transmitted from the l^{th} sub-block, denoted as $\mathcal{A}_l = \left\{a_{(l-1)p_I+1}, a_{(l-1)p_I+2}, \ldots, a_{lp_I}\right\}$, where $l = 1, .., L$. In each group, the initial p_s bits denote the subcarrier index, selecting one active subcarrier from $N_s = 2^{p_s}$ subcarriers. The subsequent p_t bits represent the time slot index, selecting one active time slot from $N_t = 2^{p_t}$ time slots. The following p_r bits are the reference indices that determine one of the reference-chaotic signals $X_{q,k}$, with $q = 1, .., N_r$ and $N_r = 2^{p_r}$. The final bit, p_m, is the modulated bit. There are $2^v + 1$ subcarriers, where v is an intege $v \geq p_s$. The first subcarrier transmits the chaotic reference signals $X_n(t)$, with $n = 1, .., \beta$, whereas the remaining subcarriers are divided into $L = 2^v/N_s$ sub-blocks. A bits-to-symbol converter transforms the subcarrier index bits p_s into an index symbol, $IS_l \in \{1, .., N_s\}$, with $l = 1, .., L$ which selects a single subcarrier in the group. The lth time index $IT_l \in \{1, .., N_t\}$ is derived from the p_t bits by selectin a single time slot from the group. The p_r bits in the lth group are converted into reference index $IR_l \in \{1,.., N_r\}$, determining a single-reference chaotic signal from a set of N_r orthogonal signals, that is, $x_k^l = X_{IR_l,k}$. The modulated bit in the lth subblock is mapped into the bipolar form $b_l \in \{1, -1\}, l = 1, .., L$, using a polarity converter function. It is then transmitted by both the subcarrier indexed by IS_l and the slot indexed by IT_l through a specific reference chaotic signal indexed by IR_l using DCSK modulation.

Using the reference inde p_r, the reference index mapper of the L^{th} sub-block in Fig. 1 selects one orthogonal reference-chaotic signal to produce $x_k^l = X_{IR_l,k}$, with $k = 1, .., R$. Subsequently, the information and carrier signal mapper generates the lth 3D matrix $\boldsymbol{C}_l = [c_{i,j,1}^l, .., c_{i,j,R}^l]$, with $i = 1, .., N_t$ and $j = 1, .., N_s$ ($\boldsymbol{C}_l \in \mathbb{R}^{N_t \times N_s \times R}$), where $\boldsymbol{c}_{i,j,k}^l$ contain $X_{IR_l,k}$, with $k = 1, .., R$, if $i = IT_l$ and $j = IS_l$ or zero vector 0_k of length R otherwise,

$$\boldsymbol{c}_{i,j,k}^l = \begin{cases} X_{IR_l,k} & \text{if } i = IT_l \text{ and } j = IS_l \\ 0_k & \text{otherwise} \end{cases} \tag{2}$$

TABLE 1. Mapping example for the JSTRIM-DCSK-I system with $v = 3, p_s = 2, p_r = p_t = 1$.

lth group	Time slot index Bits/IT_l	Subcarrier - Index Bits/IS_l	Reference index Bits/IR_l	Modulated-Bit	Information-bearing matrix	Active Center Time/Frequency
1	0/1	00/1	0/1	0	$\begin{bmatrix} C^1_{1,n} \\ C^1_{2,n} \\ C^1_{3,n} \\ C^1_{4,n} \end{bmatrix} = \begin{bmatrix} -X_{1,k} & 0_k \\ 0_k & 0_k \\ 0_k & 0_k \\ 0_k & 0_k \end{bmatrix}$	t_1/f_2
2	1/2	10/3	1/2	1	$\begin{bmatrix} C^2_{1,n} \\ C^2_{2,n} \\ C^2_{3,n} \\ C^2_{4,n} \end{bmatrix} = \begin{bmatrix} 0_k & 0_k \\ 0_k & 0_k \\ 0_k & X_{2,k} \\ 0_k & 0_k \end{bmatrix}$	t_2/f_8

The signals $\boldsymbol{c}^l_{i,j,k}$ can be concatenated in the form $\boldsymbol{c}^l_{j,n} = [\boldsymbol{c}^l_{1,j,k}, \ldots, \boldsymbol{c}^l_{N_t,j,k}]$, with $n = 1, .., \beta$, multiplied by $d_{l,j}$, where $j = 1, .., N_s$, in subsequent steps. The subcarrier index mapper produces the sequence $d_{l,j}$ in the lth group, which has either modulated bits b_l, if $j = IS_l$ bits, or zero otherwise,

$$d_{l,j} = \begin{cases} b_l & if\, j = IS_l \\ 0 & \text{otherwise} \end{cases} \tag{3}$$

For JSTRIM-DCSK-I, where $N = 1$, the signals $\boldsymbol{c}^l_{j,n}$ are multiplied by $d_{l,j}$ to yield the information-bearing signals $\varphi^l_{j,n} = c^l_{j,n} d_{l,j}$ for the lth group. This results in only one nonzero vector among $N_s N_t$ vectors in each group. Table 1 provides examples of mapping functions for scenarios where $v = 3$, $p_s = 2$, $p_t =$, and $p_r = 1$. The setup consists of two sub-blocks, with four subcarrier index mappers, two time slot index mappers, and two reference index mappers for the sub-blocks. Given that the data bits for the two sub-blocks are $\mathcal{A} = \{0\,0\,0\,0\,0\,1\,0\,1\,1\,1\}$, the total bits transmitted during a single-symbol duration Lp_I, amounts to 10 bits. The reference-chaotic signals are represented as $X_n = \left[X_{1,k}, X_{2,k}\right]$, whereas the information-bearing signals are $\{d_{l,j} c^l_{j,n}\}$, with j = {1,2,3,4}. The pattern frequencies for the 1st and 2nd group are $\{f_2, f_3, f_4, f_5\}$ and $\{f_6, f_7, f_8, f_9\}$, respectively. The active center frequencies for the first and second sub-blocks are f_2 and f_8, respectively. Notably, the frequency pattern starts from the second frequency because the first frequency is reserved for transmitting the reference chaotic signal.

Within each group, the information- and reference-chaotic signals can be modulated using discrete cosine transform. The total transmitted signal is the

$$s(t) = \sum_{l=1}^{L} \sum_{j=1}^{N_s} \varphi^l_j(t) cos\left(2\pi f_{(l-1)N_s+j+1} t + \theta_{(l-1)N_s+j+1}\right) + X(t) \cos\left(2\pi f_1 t + \theta_1\right), \tag{4}$$

where $\varphi^l_j(t) = c^l_j(t)\, d_{l,j}$, $f_{(l-1)N_s+j+1}$ and $\theta_{(l-1)N_s+j+1}$ are the center frequency and phase angle of the j^{th} frequency in the l^{th} group, respectively. $X(t)$ and $c^l_j(t)$ represent the analog signals of the reference-chaotic and information-bearing signals, respectively, converted to analog signals using a square root raised-cosine pulse-shaping filter (PSF) [42]

$$X(t) = \sum_{n=1}^{\beta} X_n h(t - nT_c), n = 1, .., \beta$$
$$\varphi^l_j(t) = \sum_{n=1}^{\beta} \varphi^l_{j,n} h(t - nT_c), j = 1, .., N_s \tag{5}$$

where T_c is the interval of the chaotic samples and $h(t)$ is the normalized impulse response of the PSF with a roll-off factor ϕ, $0 < \phi \leq 1$.

Fig. 2 illustrates the receiver architecture of the JSTRIM-DCSK-I system, with the reception signals accounting for multipath propagation and noise [44], [47]

$$r(t) = \sum_{\rho=1}^{P} \alpha_\rho \delta\left(t - \tau_\rho\right) \circledast s(t) + \eta(t), \tag{6}$$

where P represents the number of propagation paths, α_ρ and τ_ρ the gain and delay for the ρth path, $\circledast$ is the convolution operation, and $\eta(t)$ is the wideband AWGN nosie with zero mean and a variance of $N_0/2$. The propagation gains α_ρ are independent random variables that follow the Rayleigh distribution. The received signal $r(t)$ is demodulated by multiplying it with $2^v(+1)$ synchronous sinusoidal subcarrier, and then processed through matched filters to obtain the jth received signal from all subcarriers with time spacing $= nTc$, $r_{j,n}, j = 1, \ldots, (2^v + 1)$ and $n = 1, \ldots, \beta$.

The discrete received signals consist of two parts. The first part is the reference chaotic signal $r_{1,n}$, where$n = 1, .., \beta$. This signal is centered at the first subcarrier and contains the N_r received reference chaotic signals. The second part is the information-bearing signal centered at frequencies $j = 2, \ldots, 2^v + 1$, represented by $r_{j,n}$. The information-bearing signals are grouped into L sub-blocks, with each sub-block containing N_s vectors. For example, the first sub-block contains signals $r_{2,n}, \ldots, r_{2+N_s,n}$, and the second sub-block contains signals $r_{3+N_s,n}, \ldots, r_{3+2N_s,n}$ and so on. These received signals are then framed into N_t vectors, each of length R, denoted as $r_{j,i,R}$, where $j = 1, .., 2^v + 1$ and $i = 1, ..N_t$. The i^{th} received reference-chaotic signals $r_{1,i,R}$ are arranged in a matrix $\mathbf{A}$ of dimensions $N_r \times R$,

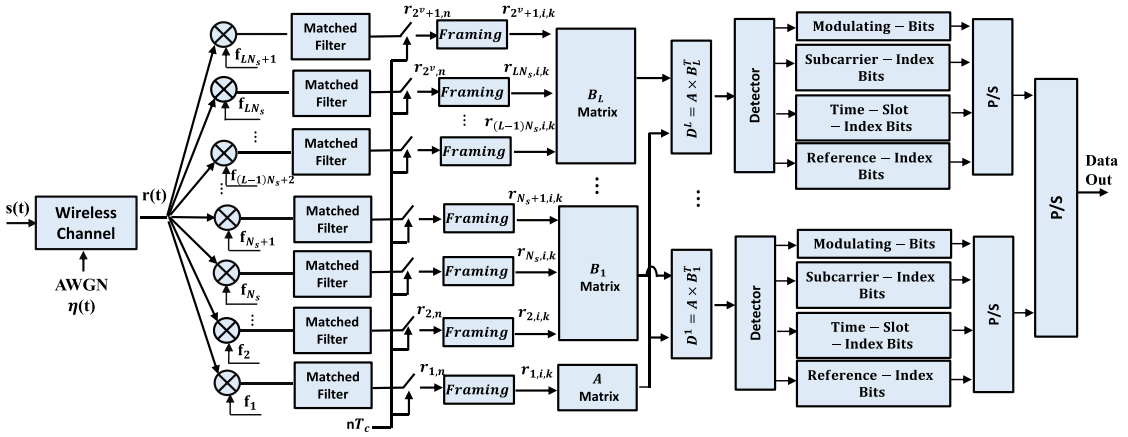

FIGURE 2. JSTRIM-DCSK receiver.

constructed as

$$\boldsymbol{A} = \begin{bmatrix} r_{1,1,1} & r_{1,1,2} & \cdots & r_{1,1,R} \\ r_{1,2,1} & r_{1,2,2} & \cdots & r_{1,2,R} \\ \vdots & \vdots & \vdots & \vdots \\ r_{1,N_r,1} & r_{1,N_r,2} & \cdots & r_{1,N_r,R} \end{bmatrix}. \quad (7)$$

In the lth sub-block, the received information-bearing signals are arranged in matrices $\boldsymbol{B}^l_{N_sN_t\times R}$ with dimensions $N_sN_t \times R$:

$$\boldsymbol{B}_l = \begin{bmatrix} r_{(l-1)N_s+2,1,1} & r_{(l-1)N_s+2,1,2} & \cdots & r_{(l-1)N_s+2,1,R} \\ \vdots & \vdots & \ddots & \vdots \\ r_{(l-1)N_s+2,N_t,1} & \vdots & \cdots & r_{(l-1)N_s+2,N_t,R} \end{bmatrix}. \quad (8)$$

The lth correlation matrices $\boldsymbol{D}^l_{N_sN_t\times N_r}$ are calculated as

$$\boldsymbol{D}^l = \boldsymbol{A} \times \boldsymbol{B}^T_l, \text{ with } l = 1, .., L. \quad (9)$$

The superscript 'T' denotes the transpose operation. The lth matrix $\boldsymbol{D}^l$ is then rearranged to obtain the variables $D^l_{i,j,q}$, where $i \in \{1, .., N_t\}$, $j \in \{1, .., N_s\}$ and $q \in \{1, .., N_r\}$ for $l = 1, .., L$. The decision variables $D^l_{i,j,q}$ are expressed for the different cases:

Case 1: For i = IT_l, $j = IS_l$ and $q = IR_l$

$$D^l_{IT_l,IS_l,IR_l} = \sum_{k=1}^{R}\left(\sum_{\rho=1}^{P}\alpha_\rho x_{IR_l,k-\tau_\rho} b_l + \eta_{IT_l,IS_l,k}\right) \times \left(\sum_{\rho=1}^{P}\alpha_\rho x_{IR_l,k-\tau_\rho} + \eta_{IT_l,1,k}\right) = D_1, \quad (10)$$

where $\eta_{i,j,k}$ are the k^{th} sample of the AWGN signal at the i^{th} time slot and j^{th} subcarrier with zero mean and standard deviation $\sqrt{N_0/2}$.

Case 2: For $i = IT_l, j = IS_l$, and $q = 1, .., N_r, q \neq IR_l$

$$D^l_{IT_l,IS_l,q} = \sum_{k=1}^{R}\left(\sum_{\rho=1}^{P}\alpha_\rho x_{IR_l,k-\tau_\rho} b_l + \eta_{IT_l,IS_l,k}\right) \times \left(\sum_{\rho=1}^{P}\alpha_\rho x_{q,k-\tau_\rho} + \eta_{q,1,k}\right) = D_2, \quad (11)$$

where $\eta_{q,1,k}$ is the k^{th} sample of the AWGN signal at q^{th} time slot and the first subcarrier, as $N_t = N_r$ and the first subcarrier holds the reference chaotic signal.

Case 3: $i = 1,.., N_t, i \neq IT_l, j = 1,.., N_s, j \neq IS_l, q = 1,.., N_r$

$$D^l_{i,j,q} = \sum_{k=1}^{R}\left(\eta_{i,j,k}\right)\left(\sum_{\rho=1}^{P}\alpha_\rho x_{q,k-\tau_\rho} + \eta_{i,1,k}\right) = D_3. \quad (12)$$

The indices of the active time, frequency, and reference in the l^{th} group are recovered using the maximum absolute values of $D^l_{i,j,q}$ for $i = 1, .., N_t, j = 1, .., N_s$ and $q = 1, .., N_r$, and can be expressed as

$$\left(\hat{IS}_l, \hat{IT}_l, \hat{IR}_l\right) = \arg \max_{\substack{i=1,...,N_t \\ j=1,...,N_s, \\ q=1,...,N_r}} \left(\left|D^l_{i,j,q}\right|\right), \text{ with } l = 1, .., L, \quad (13)$$

where $\hat{IS}_l, \hat{IT}_l$ and $\hat{IR}_l$ are the l^{th} estimated indices of the active subcarrier, time slot, and reference, respectively. The l^{th} estimated index bits are found by converting $\hat{IS}_l, \hat{IT}_l$ and $\hat{IR}_l$ into binary bits using a decimal-to-binary converter after subtracting by one, denoted as $\hat{a}_{(l-1)p_I+1}, \hat{a}_{(l-1)p_I+2}, \ldots, \hat{a}_{lp_I-1}$. The l^{th} detected modulated bit can be recovered as

$$\hat{a}_{lp_I} = \begin{cases} 0 & \text{if } sign\left(D^l_{\hat{IS}_l,\hat{IT}_l,\hat{IR}_l}\right) = -1 \\ 1 & \text{if } sign\left(D^l_{\hat{IS}_l,\hat{IT}_l,\hat{IR}_l}\right) = +1 \end{cases} \quad l = 1, .., L. \quad (14)$$

B. THE JSTRIM-DCSK-II SCHEME

The transmission and reception aspects of the second proposed, JSTRIM-DCSK-II, system are also represented by Fis. 1 and 2, respectively. Each sub-block in this system consists of $N_sN_t - 1$ active pairs of subcarriers and time slots, with one single inactive pair selected by the subcarrier and time slot pair. Each group has $p_{II} =$

TABLE 2. Mapping example for the JSTRIM-DCSK-II system with $v = 2, p_s = 2, p_r = p_t = 1$.

lth group	*Time slot index Bits/IT_l*	*Subcarrier-Index Bits/IS_l*	*Reference index Bits/$IR_{i,j,l}$*	*Modulated-Bit/bipolar*	*Information-bearing Matrix*	*Active Center Time/Frequency*
1	*0/1*	*00/1*	$\begin{bmatrix} - & 0/1 \\ 0/1 & 1/2 \\ 0/1 & 1/2 \\ 1/2 & 1/2 \end{bmatrix}$	$\begin{bmatrix} - & 0/-1 \\ 0/-1 & 0/-1 \\ 1/1 & 1/1 \\ 1/1 & 1/1 \end{bmatrix}$	$\begin{bmatrix} C^1_{1,n} \\ C^1_{2,n} \\ C^1_{3,n} \\ C^1_{4,n} \end{bmatrix} = \begin{bmatrix} \mathbf{0_k} & -X_{1,k} \\ -X_{1,k} & -X_{2,k} \\ X_{1,k} & X_{2,k} \\ X_{2,k} & X_{2,k} \end{bmatrix}$	t_1/f_2
2	*1/2*	*11/4*	$\begin{bmatrix} 1/2 & 1/2 \\ 0/1 & 0/1 \\ 0/1 & 1/2 \\ 1/2 & - \end{bmatrix}$	$\begin{bmatrix} 1/1 & 1/1 \\ 1/1 & 0/-1 \\ 1/1 & 1/1 \\ 0/-1 & - \end{bmatrix}$	$\begin{bmatrix} C^2_{1,n} \\ C^2_{2,n} \\ C^2_{3,n} \\ C^2_{4,n} \end{bmatrix} = \begin{bmatrix} X_{2,k} & X_{2,k} \\ X_{1,k} & -X_{1,k} \\ X_{1,k} & X_{2,k} \\ -X_{2,k} & \mathbf{0_k} \end{bmatrix}$	t_2/f_9

$((N_sN_t - 1)(p_r + 1) + p_s + p_t)$ bits, where the number of active pairs in each group is $N = (N_sN_t - 1)$, and only a single inactive pair is chosen by the subcarrier and time slot pair. The total number of transmitted bits are Lp_{II} bits. For each symbol period, the lth transmitted bits are $\mathcal{A}_l = \{a_{(l-1)p_{II}+1}, a_{(l-1)p_{II}+2}, \ldots, a_{lp_{II}}\}$, $l = 1, .., L$. For each group, the first p_s bits are subcarrier index bits that select a single null subcarrier from N_s subcarriers. The second p_t bits are time slot index bits that select a single active time slot from $N_t = 2^{p_t}$ time slots. The third $(N_sN_t - 1)\,p_r$ packet bits are reference index packet bits that select reference-chaotic signals $(X_{q,k}, q = 1, .., N_r)$ for each active (subcarrier and time slot) pair, where $N_r = 2^{p_r}$. The final p_m bits, ranging form $m = 1$ to $(N_sN_t - 1)$ serve as modulated bits, with one bit allocated to each pair of subcarriers and time slots.

In this system, the reference index mapper in the lth group selects the orthogonal reference-chaotic signal out of $N = (N_sN_t - 1)$ possibilities, using the p_r bits to generate $x^l_{i,j,k} = X_{IR^l_{i,j},k}$ for $k = 1, .., R$, $l = 1, .., L$, $i = 1, .., N_t$, $j = 1, .., N_s$ and $i \neq IT_l$ and $j \neq IS_l$. The information and carrier signal mapper generates the lth 3D matrix $\boldsymbol{C}_l = [c^l_{i,j,1}, .., c^l_{i,j,R}]$ with $i = 1, .., N_t$ and $j = 1, .., N_s$ ($\boldsymbol{C}_l \in \mathbb{R}^{N_t \times N_s \times R}$)

$$\boldsymbol{c}^l_{i,j,k} = \begin{cases} 0_k & if\ i = IT_l and j = IS_l \\ X_{IR^l_{i,j},k} & if\ i \neq IT_l, j \neq IS_l, \end{cases} \quad k = 1, .., R. \tag{15}$$

The signals $\boldsymbol{c}^l_{i,j,k}$ are then multiplied by the lth packet data bits $d^l_{i,j}$. This operation results in either a zero value in the subcarrier index selected by p_s and the time slot index selected by p_t, or the values of the modulated bits $b^l_{i,j} = [a_{(l-1)p_{II}+p_{II}-(N_sN_t-1)}..a_{p_{II}+(l-1)p_{II}}]$:

$$d^l_{i,j} = \begin{cases} b^l_{i,j} & if\ i = 1, .., N_t, i \neq IT_l, j = 1, .., N_s, j \neq IS_l \\ 0 & if\ i = IT_l, j = IS_l. \end{cases} \tag{16}$$

The lth multiplied signals $\varphi^l_{i,j,k} = d^l_{i,j}\boldsymbol{c}^l_{i,j,k}$, are transformed into signals $\varphi^l_{j,n}$, where n = 1,.., β and j = 1,.., N_s, using the concatenating function $\varphi^l_{j,n} = [\varphi^l_{1,j,k}\varphi^l_{2,j,k} \ldots \varphi^l_{N_t,j,k}]$. Therefore, among $N_s \times N_t$ sequences, in each grou, there is one zero-value sequence that carries the subcarrier and time slot index bits and N sequences that carry the reference index and information data bits. Table 2 presents a simple mapping example for $v = 3$, $p_s = 2$, $p_t = 1$, and $p_r = 1$. There are two sub-blocks, four subcarrier index mappers, two time slot index mappers, and seven packets from the two reference index mappers. Assuming that the data bits for the two sub-blocks are $\mathcal{A} = \{00\ 0\ 0010111\ 0001111\ 11\ 1\ 1100011\ 1110110\}$, the total number of bits for one symbol duration $Lp_{II} = 34$ bits. The reference-chaotic signals $X_n = [X_{1,k}, X_{2,k}]$ and the information-bearing signals are $d^l_{i,j}c^l_{i,j,k}$, $i = 1,2$, with $j \in \{1, 2, 3, 4\}$. The pattern subcarriers for the 1st and 2nd group are $\{f_2, f_3, f_4, f_5\}$ and $\{f_6, f_7, f_8, f_9\}$, respectively. The inactive center frequencies for each group are f_2 and f_9 for the first and second sub-blocks, respectively. In addition, the inactive center times for each group are t_1 and t_2 for the first and second grou, respectively.

In the JSTRIM-DCSK-II system, the values of the lth decision variable $D^l_{i,j,q}$, where i = 1,.., N_t, j = 1,.., N_s, and $q = 1, .., N_r$ are expressed according to the following cases:

Case 1: For $i \neq IT_l, j \neq IS_l$ and $q = IR_l$

$$D^l_{i,j,IR_l} = \sum_{k=1}^{R}\left(\sum_{\rho=1}^{P}\alpha_\rho x_{IR^l_{i,j},k-\tau_\rho}b_l + \eta_{i,j,k}\right) \times \left(\sum_{\rho=1}^{P}\alpha_\rho x_{IR_l,k-\tau_\rho} + \eta_{IR_l,1,k}\right) = D_4, \tag{17}$$

Case 2: For $i \neq IT_l, j \neq IS_l and q \neq IR_l$

$$D^l_{i,j,q} = \sum_{k=1}^{R}\left(\sum_{\rho=1}^{P}\alpha_\rho x_{IR_l,k-\tau_\rho}b_l + \eta_{IT_l,IS_l,k}\right) \times \left(\sum_{\rho=1}^{P}\alpha_\rho x_{q,k-\tau_\rho} + \eta_{q,1,k}\right) = D_5, \tag{18}$$

Case 3: $i = IT_l, j = IS_l$

$$D^l_{IT_l,IS_l,q} = \sum_{k=1}^{R}\left(\eta_{IT_l,IS_l,k}\right)\left(\sum_{\rho=1}^{P}\alpha_\rho x_{q,k-\tau_\rho} + \eta_{q,1,k}\right) = D_6. \tag{19}$$

To recover the transmitted bits from the decision variables, the following steps are performed:

1. Compute the sum of the absolute value of $D^l_{i,j,q}$ for $q = 1, .., N_r$ and $l = 1, .., L$ to get

$$Z^l_{i,j} = \sum_{q=1, q\neq IR_l}^{N_r} \left|D^l_{i,j,q}\right| + \left|D^l_{i,j,IR_l}\right|, \tag{20}$$

where $Z^l_{i,j}$ is the sum of the absolute decision variables in the lth subblock, ith time slot, and jth subcarrier, respectively.

2. The lth recovered index of the frequency and time slot is detected by taking the minimum value of $Z^l_{i,j}$ for $i = 1, .., N_t$ and $j = 1, .., N_s$, expressed as

$$\left(\hat{IS}_l, \hat{IT}_l\right) = \arg \min_{\substack{i=1,\ldots,N_t \\ j=1,\ldots,N_s}} \left(Z^l_{i,j}\right), \tag{21}$$

where $\hat{IS}_l, \hat{IT}_l$ are the lth estimated index subcarrier and index timeslot, respectively.

3. The estimated reference index in the lth group was determined from the maximum absolute value of $D^l_{i,j,q}$ for $q = 1, .., N_r$ and $l = 1, .., L$, expressed as

$$[\sim, IN^l_{i,j}] = \max_{q=1,\ldots,N_r} \left(\left|D^l_{i,j,q}\right|\right), \tag{22}$$

and by reshaping the indices $IN^l_{i,j}$:

$$\hat{IR}_{l,m} = IN^l_{i,j}, \text{ for } i \neq IT_l, j \neq IS_l. \tag{23}$$

4. The recovered index bits of the lth group are obtained by converting $\hat{IS}_l, \hat{IT}_l$ and $\hat{IR}_{l,m}$ into binary bits using a decimal-to-binary converter after subtraction by one, $[\hat{a}_{(l-1)p_{II}+1}, \ldots, \hat{a}_{(l-1)p_{II}+p_s}]$, $[\hat{a}_{(l-1)p_{II}+p_s+1}, \ldots, \hat{a}_{(l-1)p_{II}+p_s+p_t}]$, $[\hat{a}_{(l-1)p_{II}+p_s+p_t+1}, \ldots, \hat{a}_{(l-1)p_{II}+p_s+p_t+Np_r}]$, respectively.

5. In the final step, the detected modulated bits in the lth group can be estimated as

$$\hat{a}_{(l-1)p_{II}+p_s+p_t+Np_r+m} = \begin{cases} 0 & if\ sign\left(Z^l_{i,j}\right) = -1 \\ 1 & if\ sign\left(Z^l_{i,j}\right) = +1 \end{cases}, \text{ for } i \neq IT_l, j \neq IS_l, \tag{24}$$

and $l = 1, .., L, m = 1, .., N, i = 1, .., N_t$ and $j \neq IS_l$.

III. BER PERFORMANCE ANALYSIS

In this section, we present an in-depth analysis of the performance of the JSTRIM-DCSK system, focusing on energy efficiency metrics and including dynamic bit rate (DBR), bandwidth efficiency, complexity analysis, and bit error rate (BER). Our analysis assumes a slowly fading Rayleigh channel, with a symbol duration that significantly surpasses the maximum multipath delay ($0 < \tau_{max} \ll$ R). Consequently, we disregard inter-symbol interference (ISI) in alignment with established practices [28], [44].

A. BIT ERROR RATES OF JSTRIM-DCSK-I SYSTEMS

To maintain generality, if the lth modulated bit $b_l = +1$, Equations (10), (11), and (12) can be simplified as follows to derive the first three decision variables:

$$\begin{aligned} D_1 = &\sum_{k=1}^{R}\sum_{\rho=1}^{P} \alpha_\rho^2 x^2_{IR_l,k-\tau_l} \\ &+ \sum_{k=1}^{R}\sum_{\rho=1}^{P} \alpha_\rho x_{IR_l,k-\tau_l}\eta_{IT_l,1,k} \\ &+ \sum_{k=1}^{R}\sum_{\rho=1}^{P} \alpha_\rho x_{IR_l,k-\tau_l}\eta_{IT_l,IS_l,k} \\ &+ \sum_{k=1}^{R} \eta_{IT_l,IS_l,k}\eta_{IT_l,1,k}, \end{aligned} \tag{25}$$

$$\begin{aligned} D_2 = &\sum_{k=1}^{R}\sum_{\rho=1}^{P} \alpha_\rho^2 x_{IR_l,k-\tau_\rho} x_{q,k-\tau_l} \\ &+ \sum_{k=1}^{R}\sum_{\rho=1}^{P} \alpha_\rho x_{IR_l,k-\tau_\rho}\eta_{q,1,k} \\ &+ \sum_{k=1}^{R}\sum_{\rho=1}^{P} \alpha_\rho x_{q,k-\tau_\rho}\eta_{IT_l,IS_l,k} \\ &+ \sum_{k=1}^{R} \eta_{IT_l,IS_l,k}\eta_{q,1,k}, \end{aligned} \tag{26}$$

$$\begin{aligned} \mathrm{D_3} = &\sum_{\mathrm{k=1}}^{\mathrm{R}}\sum_{\rho=1}^{\mathrm{P}} \alpha_\rho \mathrm{x_{q,k-\tau_\rho}}\eta_{\mathrm{i,j,k}} \\ &+ \sum_{\mathrm{k=1}}^{\mathrm{R}} \eta_{\mathrm{i,j,k}}\eta_{\mathrm{i,1,k}}. \end{aligned} \tag{27}$$

The first term in (26) is zero because both $x_{IR_l,k}$ and $x_{q,k}$ are orthogonal signals, $\sum_{k=1}^{R} x_{IR_l,k-\tau_l} x_{q,k-\tau_l} \approx 0$ for $IR_l \neq q$. The means and variances of the decision variables $D_1, D_2,$ and D_3 can be approximated as

$$\begin{aligned} &E(D_1) \approx R\sum_{\rho=1}^{P} \alpha_\rho^2 E\left[x^2_{IR_l,k}\right] = \mu_1, \\ &E(D_2) \approx 0 = \mu_2, \\ &E(D_3) \approx 0 = \mu_3 \text{ and} \end{aligned} \tag{28}$$

$$\begin{aligned} &Var(D_1) \approx R\sum_{\rho=1}^{P} \alpha_\rho^2 E\left[x^2_{IR_l,k}\right] N_0 + R\frac{N_0^2}{4} = \sigma_1^2, \\ &Var(D_2) \approx R\sum_{\rho=1}^{P} \alpha_\rho^2 E\left[x^2_{IR_l,k}\right] N_0 + R\frac{N_0^2}{4} = \sigma_2^2, \\ &Var(D_3) \approx R\sum_{\rho=1}^{P} \alpha_\rho^2 E\left[x^2_{IR_l,k}\right] \frac{N_0}{2} + R\frac{N_0^2}{4} = \sigma_3^2, \end{aligned} \tag{29}$$

where E(.) and $Var(.)$ denote the expectation and variance operations, respectively. Let the bit energy of JSTRIM-DCSK-I be $E_b^I = R\,(L + N_r)\,E\left[x^2_{IR_l,k}\right]/Lp_I$ and the bit signal-to-noise ratio be $\gamma_b^I = E_b^I \sum_\rho^P \alpha_\rho^2/N_0$. Equations (28) and (29) are rewritten in terms of γ_b^I as

$$\mu_1 = N_0 \frac{Lp_I \gamma_b^I}{(L + N_r)}, \tag{30}$$

$$\sigma_1^2 = \mathrm{N_0^2}\left(\frac{\mathrm{Lp_I\Gamma_b^I}}{\mathrm{(L+N_r)}} + \frac{\mathrm{R}}{4}\right) = \sigma_2^2, \tag{31}$$

$$\sigma_3^2 = \mathrm{N_0^2}\left(\frac{\mathrm{Lp_I\Gamma_b^I}}{\mathrm{2(L+N_r)}} + \frac{\mathrm{R}}{4}\right). \tag{32}$$

The BER theory of JSTRIM-DCSK-I, P_{BER-I}, is a function of the BER of the index bits (subcarrier, time slot, and reference index bits), $P_{index-I}$ and the BER of the

modulated bits, P_{mod-I}. The overall BER of the JSTRIM-DCSK_I system is given by

$$P_{BER-I} = \frac{1}{p_I} P_{mod-I} + \frac{p_s + p_t + p_r}{p_I} P_{index-I}. \quad (33)$$

1) BER OF REFERENCE INDEX BITS ($P_{index-I}$)

Faults occur if $|D_{IT,IS,IR}|$ is smaller than the maximum absolute value of the decision variable for the erroneous index $|D_{i,j,q}|, i \in \{1,..,N_t\}, i \neq IT, j \in \{1,..,N_s\}, j \neq IS, q \in \{1,..,N_r\}$, q $\neq IR$. There are $N_r(N_tN_s-1)$ independent correlator outputs with identical distributions that are used for the subcarrier time index detection. Similarly, for reference index detection, there are $(N_r - 1)$ independent correlator outputs with identical distributions, all representing the error values. The Symbol Error Rate (SER) of the index bits is given by [36], [38], [44]:

$$\begin{aligned} &P_{SER-index-I} \\ &= Pr\left[|D_{IT,IS,IR}| < max\left(\left|D_{i,j,q}\right|\right)\right] \\ &= 1 - \int_0^{+\infty} \left(F_{|D_3|}\left(y, \mu_3, \sigma_3^2\right)\right)^{N_r(N_tN_s-1)} \\ &\quad \times \left(F_{|D_2|}\left(y, \mu_2, \sigma_2^2\right)\right)^{(N_r-1)} f_{|D_1|}\left(y, \mu_1, \sigma_1^2\right) dy, \end{aligned} \quad (34)$$

where $F_{|D_3|}\left(y, \mu_3, \sigma_3^2\right)$, $F_{|D_2|}\left(y, \mu_2, \sigma_2^2\right)$ and $f_{|D_1|}\left(y, \mu_1, \sigma_1^2\right)$ are the cumulative distribution functions (CDF) of $\left|D_{i,j,q}\right|, i = 1,..,N_t, i \neq IT, j = 1,..,N_s, j \neq IS, q = 1,..,N_r$, CDF of $\left|D_{IT,IS,q}\right|, q = 1,..,N_r, q \neq IR$ and probability density function (PDF) of $\left|D_{IT,IS,IR}\right|$, respectively. These follow a folded normal distribution and are calculated as follows [36], [38], [44]:

$$\begin{aligned} &F_{|D_3|}\left(y, \mu_3, \sigma_3^2\right) \\ &= erf\left(\frac{y - \mu_3}{\sqrt{2\sigma_3^2}}\right), \end{aligned} \quad (35)$$

$$\begin{aligned} &F_{|D_2|}\left(y, \mu_2, \sigma_2^2\right) \\ &= erf\left(\frac{y - \mu_2}{\sqrt{2\sigma_2^2}}\right), \end{aligned} \quad (36)$$

$$\begin{aligned} &f_{|D_1|}\left(y, \mu_1, \sigma_1^2\right) \\ &= \frac{1}{\sqrt{2\pi\sigma_1^2}}\left(exp\left(-\frac{(y-\mu_1)^2}{2\sigma_1^2}\right) + exp\left(-\frac{(y+\mu_1)^2}{2\sigma_1^2}\right)\right). \end{aligned} \quad (37)$$

By substituting Equations (30) to (32) and (35) into Equation (37), and then substituting the result into Equation (34), we obtain the symbol error rate of the index bits (38), as shown at the bottom of the next page.

The relationship of $P_{SER-index-I}$ and $P_{index-I}$ can be written as:

$$P_{index-I} = \frac{2^{((p_s+p_t+p_r)-1)}}{2^{(p_s+p_t+p_r)} - 1} P_{SER-index-I}. \quad (39)$$

2) BER OF MODULATED BITS (P_{mod-I})

The BER of the modulated bits is influenced by two scenarios. In the first scenario, when the modulated bits are faulty, but all index bits are correct, the BER of the modulated bits, denoted as P_{DCSK-I}, is computed as follows:

$$\begin{aligned} \mathrm{P_{DCSK-I}} &= \frac{1}{2}\mathrm{erfc}\left[\left(\frac{2\sigma_1^2}{\mu_1^2}\right)^{-\frac{1}{2}}\right] \\ &= \frac{1}{2}\mathrm{erfc}\left[\left(\frac{2(\mathrm{L}+\mathrm{N_r})}{\mathrm{Lp_I}\Gamma_\mathrm{b}^\mathrm{I}} + \frac{\mathrm{R}}{2}\frac{(\mathrm{L}+\mathrm{N_r})^2}{\mathrm{L}^2\mathrm{p_I^2}(\gamma_\mathrm{b}^\mathrm{I})^2}\right)^{-\frac{1}{2}}\right]. \end{aligned} \quad (40)$$

In the second scenario, where the index bits (time slot, subcarrier and reference index bits) are faulty, resulting in the modulated bits being obtained from the incorrect correlator, the correct detection probability is approximated to 0.5. Accordingly, P_{mod-I} is calculated as follows:

$$P_{mod-I} = P_{DCSK-I}\left(1 - P_{SER-index-I}\right) + 0.5P_{SER-index-I}. \quad (41)$$

By substituting (39) and (41) into (33), the P_{BER-I} over multipath Rayleigh fading channels is derived.

B. BIT ERROR RATES OF JSTRIM-DCSK-II SYSTEMS

In JSTRIM-DCSK-II, each group utilizes $N = N_sN_t - 1$ paired subcarriers and time slots, along with a single inactive sequence, resulting in $p_{II} = (p_s + p_t + Np_r + N)$ transmitted bits and an overall number of $\mathrm{L}p_{II} = \mathrm{L}(p_s + p_t + Np_r + N)$ bits per frame. The system's bit energy and bit signal-to-noise ratio are $E_b^{II} = (LN + N_r)\sum_{k=1}^{R} x_{IR_l,k}^2 / \mathrm{L}p_{II}$ and $\gamma_b^{II} = E_b^{II}\sum_{\rho}^{P}\alpha_\rho^2/N_0$.

The mean and variance of the decision variables D_4, D_5, and D_6 in (17), (18), and (19), are identical to those of D_1, D_2, and D_3, respectively. Therefore, the mean and variance values of the variables D_4, D_5, and D_6 in terms of the bit signal-to-noise ratio γ_b^{II} are

$$\begin{aligned} &\mu_4 = N_0\frac{Lp_{II}\gamma_b^{II}}{(LN+N_r)}, \sigma_4^2 = N_0^2\left(\frac{Lp_{II}\gamma_b^{II}}{(LN+N_r)} + \frac{R}{4}\right), \\ &\mu_5 = 0, \sigma_5^2 = N_0^2\left(\frac{Lp_{II}\gamma_b^{II}}{(LN+N_r)} + \frac{R}{4}\right), \text{ and} \\ &\mu_5 = 0, \sigma_6^2 = N_0^2\left(\frac{Lp_{II}\gamma_b^{II}}{2(LN+N_r)} + \frac{R}{4}\right). \end{aligned} \quad (42)$$

The BER of the JSTRIM-DCSK-II system combines the BERs of the subcarrier time index bits, reference index bits,

and modulated bits, expressed as

$$P_{BER-II} = \frac{N}{p_{II}} P_{mod-II} + \frac{Np_r}{p_{II}} P_{RI-II} + \frac{p_s + p_t}{p_{II}} P_{STI-II}. \tag{43}$$

1) BER OF REFERENCE INDEX BITS (P_{RI-II})

Faults occur if $|D_{i,j,IR}|$ is smaller than the maximum absolute value of the decision variable for erroneous index bits $|D_{i,j,q}|, q = 1, .., N_r, q \neq IR_l, i = 1, .., N_t, i \neq IT_l, j = 1,.., N_s, j \neq IS_l$. The SER of the reference index bits is determined by [37], [39], [44]:

$$\begin{aligned} P_{SER-RI-II} &= Pr\left[\left|D_{i,j,IR_l}\right| < max\left(\left|D_{i,j,q}\right|\right)\right] \\ &= 1 - \int_0^{+\infty} \left(F_{|D_{i,j,q}|}\left(y, \mu_5, \sigma_5^2\right)\right)^{N_r - 1} \\ &\quad \times f_{|D_{i,j,IR_l}|}\left(y, \mu_4, \sigma_4^2\right) dy, \end{aligned} \tag{44}$$

where $F_{|D_{i,j,q}|}\left(y, \mu_5, \sigma_5^2\right)$ and $f_{|D_{i,j,IR_l}|}\left(y, \mu_4, \sigma_4^2\right)$ are the cumulative distribution function (CDF) of $\left|D_{i,j,q}\right|, q = 1, .., N_r, q \neq IR_l$, and the probability density function (PDF) of $\left|D_{i,j,IR_l}\right|$, respectively. Theses follow a folded normal distribution [36], [38], [44]. After substituting the appropriate expressions and rearranging the terms, the SER of the reference index bits can be expressed as (45), as shown at the bottom of the next page, and the BER of the reference index bits is

$$P_{RI-II} = \frac{2^{(p_r - 1)}}{2^{p_r} - 1} P_{SER-RI-II}. \tag{46}$$

2) BER OF SUBCARRIER TIME INDEX BITS (P_{STI-II})

The mean and variance of the decision variables $|D_\delta|$, where $\delta = \{4, 5, 6\}$, follow a folded Gaussian distribution [45], [50] and are calculated as

$$\mu_{|D_\delta|} = \sqrt{\frac{2\sigma_\delta^2}{\pi}} e^{-\frac{\mu_\delta^2}{2\sigma_\delta^2}} - \mu_\delta erf\left(\frac{-\mu_\delta}{\sqrt{2\sigma_\delta^2}}\right) \tag{47}$$

and

$$\sigma_{|D_\delta|}^2 = \mu_\delta^2 + \sigma_\delta^2 - \mu_{|D_\delta|}^2, \delta = \{4, 5, 6\}. \tag{48}$$

Here, $\mu_{|D_4|}$, $\mu_{|D_5|}$, and $\mu_{|D_6|}$ represent the mean values and $\sigma_{|D_4|}^2$, $\sigma_{|D_5|}^2$, and $\sigma_{|D_6|}^2$ the variances of $|D_\delta|$. The mean values and variances of $Z_{i,j}^l$ are

$$\mu_{Z_{i,j}^l} = \begin{cases} (N_r - 1)\mu_{|D_5|} + \mu_{|D_4|} = \mu_7, i = 1, .., N_s, i \neq IS_l, \\ \qquad\qquad , j = 1, .., N_t, j \neq IT_l \\ N_r \mu_{|D_6|} = \mu_8, i = IS_l, j = IT_l, \end{cases} \tag{49}$$

and

$$\sigma_{Z_{i,j}^l}^2 \approx \begin{cases} (N_r - 1)\sigma_{|D_5|}^2 + \sigma_{|D_4|}^2 = \sigma_7^2, i = 1, .., N_s, i \neq IS_l, \\ \qquad\qquad j = 1, .., N_t, j \neq IT_l \\ N_r \sigma_{|D_6|}^2 = \sigma_8^2, i = IS_l, j = IT_l, \end{cases} \tag{50}$$

yielding

$$\begin{aligned} \mu_7 &= \sqrt{\frac{2N_0^2}{\pi}\left(\Omega + \frac{R}{4}\right)}\left((N_r - 1) + e^{-\Gamma}\right) \\ &\quad - N_0 \Omega \text{erf}\left(-\sqrt{\Gamma}\right), \end{aligned} \tag{51}$$

$$\mu_8 = N_r \sqrt{\frac{2N_0^2}{\pi}\left(\Omega + \frac{R}{4}\right)}, \tag{52}$$

$$\begin{aligned} \sigma_7^2 &= N_0^2\left(\Omega + \frac{R}{4}\right)\left((N_r - 1)\left(\frac{\pi - 2}{\pi}\right) + 1\right) + N_0^2\Omega^2 \\ &\quad - \left(\sqrt{\frac{2N_0^2}{\pi}\left(\Omega + \frac{R}{4}\right)} e^{-\Gamma} - N_0\left(\Omega + \frac{R}{4}\right) erf\left(-\sqrt{\Gamma}\right)\right)^2, \end{aligned} \tag{53}$$

$$\sigma_8^2 = N_r N_0^2\left(\frac{\Omega}{2} + \frac{R}{4}\right)\left(\frac{\pi - 2}{\pi}\right), \tag{54}$$

where $\Omega = \frac{Lp_{II}\gamma_b^{II}}{LN + N_r}$ and $\Gamma = \frac{2L^2 p_{II}^2 (\gamma_b^{II})^2}{4Lp_{II}\gamma_b^{II}(LN + N_r) + R(LN + N_r)^2}$. The SER of the subcarrier time index bits is calculated as [36], [44]

$$\begin{aligned} &P_{SER-STI-II} \\ &= \int_0^{+\infty} \left(1 - \left(1 - \frac{1}{2}\left(1 + erf\left(\frac{(y - \mu_7)}{\sqrt{2\sigma_7^2}}\right)\right)\right)^{N_s N_t - 1}\right) \\ &\quad \times \frac{1}{\sqrt{2\pi\sigma_8^2}}\left(e^{-\frac{(y - \mu_8)^2}{2\sigma_8^2}}\right) dy, \end{aligned} \tag{55}$$

$$\begin{aligned} P_{SER-index-I} &= 1 - \sqrt{\frac{2\left(L + N_r\right)}{\pi N_0^2\left(4Lp_I\gamma_b^I + R(L + N_r)\right)}} \int_0^{+\infty} \left(erf\left(\frac{\sqrt{2(L + N_r)}y}{\sqrt{N_0^2\left(2Lp_I\gamma_b^I + R(L + N_r)\right)}}\right)\right)^{N_r(N_tN_s - 1)} \\ &\quad \times \left(erf\left(\frac{\sqrt{2(L + N_r)}y}{\sqrt{N_0^2\left(4Lp_I\gamma_b^I + R(L + N_r)\right)}}\right)\right)^{(N_r - 1)} \\ &\quad \times \left(exp\left(-\frac{2\left((L + N_r)y - N_0 Lp_I\gamma_b^I\right)^2}{N_0^2(L + N_r)\left(4Lp_I\gamma_b^I + R(L + N_r)\right)}\right) + exp\left(-\frac{2\left((L + N_r)\,y + N_0 Lp_I\gamma_b^I\right)^2}{N_0^2(L + N_r)\left(4Lp_I\gamma_b^I + R(L + N_r)\right)}\right)\right) dy. \end{aligned} \tag{38}$$

leading to the BER of the subcarrier time index bits

$$P_{STI-II} = \frac{2^{((p_s+p_t)-1)}}{2^{(p_s+p_t)}-1} P_{SER-STI-II}. \quad (56)$$

3) BER OF MODULATED BITS (P_{mod-II})

The BER of a DCSK system $P_{DCSK-II}$ is calculated as:

$$P_{DCSK-II} = \frac{1}{2} erfc\left[\left(\frac{2\sigma_4^2}{\mu_4^2}\right)^{-\frac{1}{2}}\right] = \frac{1}{2} erfc\left[\left(\frac{2(LN+N_r)}{Lp_{II}\gamma_b^{II}} + \frac{R}{2}\frac{(LN+N_r)^2}{L^2 p_{II}^2 (\gamma_b^{II})^2}\right)^{-\frac{1}{2}}\right]. \quad (57)$$

For modulated bits, fault detection scenarios include error recovery of modulated bits and index bits, incorrect detection of reference index bits, subcarrier time index bits, and both reference and subcarrier time index bits. The BER of the modulated bits is expressed as

$$\begin{aligned} P_{mod-II} &= P_{DCSK-II}\left(1 - P_{SER-STI-II}\right)\left(1 - P_{SER-RI-II}\right) \\ &+ \frac{0.5 + P_{DCSK-II}(p_r - 1)}{p_r} \\ &\times P_{SER-RI-II}\left(1 - P_{SER-index-II}\right) \\ &+ \frac{0.5 + P_{DCSK-II}(p_s + p_t - 1)}{p_s + p_t} \\ &\times P_{SER-index-II}\left(1 - P_{SER-RI-II}\right) \\ &+ 0.5 P_{SER-RI-II} P_{SER-index-II}. \end{aligned} \quad (58)$$

Thus, the conditional probability P_{BER-II} over the MRFC can be derived. The average BER over the MRFC for JSTRIM-DCSK-I and JSTRIM-DCSK-II is obtained by integrating P_{BER-I} and P_{BER-II} over γ_b^I and γ_b^{II}:

$$P_{Rayleigh-\varepsilon} = \int_0^{+\infty} P_{BER-\varepsilon} f(\gamma_b^{\varepsilon}) d\gamma_b^{\varepsilon}, \varepsilon = \{I, II\}, \quad (59)$$

where $f(\gamma_b^{\varepsilon})$ is the PDF of γ_b^{ε}, and $\bar{\gamma}_b^{\varepsilon} = \frac{E_b^{\varepsilon}\sum_l^L E(\alpha_l^2)}{N_0}$. These expressions are also applied to derive the analytical BER of JSTRIM-DCSK-I and JSTRIM-DCSK-II over AWGN by setting $\mathcal{L} = 1$, $\tau_1 = 0$ and $\alpha_1 = 1$ in all equations.

IV. EFFICIENCY AND COMPLEXITY ANALYSIS

A. ENERGY EFFICIENCY

The symbol energy of the transmitted signal in the JSTRIM-DCSK-I system is given by

$$E_s = E_d + E_r = E_d + \frac{N_r E_d}{L} = E_d\left(\frac{L+N_r}{L}\right), \quad (60)$$

where E_d and E_r are the data and reference energy, respectively. The bit energy is given by $E_b = E_s/Lp_I$, and the ratio of the information energy to the bit energy (DBR) [29], [44] is expressed as

$$DBR_{\text{JSTRIM-DCSK-I}} = \frac{E_d}{E_b} = \frac{L^2 p_I}{(L+N_r)}. \quad (61)$$

The DBR for JSTRIM-DCSK-II is accordingly $DBR_{\text{JSTRIM-DCSK-II}} = \frac{L^2 N p_{II}}{LN+N_r}$. Comparisons of DBRs for various index-modulation-based DCSK systems are provided in Table 3, where $M = 2^v$ and v is an integer number ($v \geq p_s$), and $L = 2^{v-p_s}$. Fig. 3 compares the DBR for different DCSK modulations with various parameters versus p_s. The results indicate that the JSTRIM-DCSK-II system outperforms recent modulations across all p_s-values.

The lack of precision of DBR for energy savings in index modulation systems can be addressed by the energy saving (*Esav*) factor per sub-band, when considering that mapped bits do not require energy, as in [51]

$$E_{sav} = \left(1 - \frac{total\ modulated - bits}{total\ transmitted\ bits}\right) E_b\%. \quad (62)$$

The right column in Table 3 lists *Esav* for various index modulation aided DCSK systems and Fig. 4 compares *Esav* between proposed systems and others for different bit configurations. JSTRIM-DCSK-I exhibits superior *Esav* compared to other modulation schemes, improving with more subcarrier or time slot index bits. JSTRIM-DCSK-II competes well with the existing systems, particularly GSPIM-DCSK-II, indicating improved energy savings.

B. SPECTRAL EFFICIENCY (SE)

Assuming that the bandwidth for each subcarrier is identical and is denoted by B, the spectral efficiency SE [44], [48] of the JSTRIM-DCSK system can be defined as

$$\eta_{JSTRIM-DCSK-I} = \frac{\frac{Lp_I}{RN_t T_c}}{(2^v+1)B} = \frac{Lp_I}{N_t(M+1)RT_c B}, \quad (63)$$

$$\eta_{JSTRIM-DCSK-II} = \frac{\frac{Lp_{II}}{RN_t T_c}}{(2^v+1)B} = \frac{Lp_{II}}{N_t(M+1)RT_c B}. \quad (64)$$

$$P_{SER-RI-II} = 1 - \sqrt{\frac{2(LN+N_r)}{\pi N_0^2\left(4Lp_{II}\gamma_b^{II} + R(LN+N_r)\right)}} \int_0^{+\infty} \left(erf\left(\frac{\sqrt{2(LN+N_r)}y}{N_0\sqrt{4Lp_{II}\gamma_b^{II} + (LN+N_r)R}}\right)\right)^{N_r-1} \times \left(exp\left(-\frac{2(y(LN+N_r) - N_0 Lp_{II}\gamma_b^{II})^2}{N_0^2(4Lp_{II}\gamma_b^{II} + R(LN+N_r))}\right) + exp\left(-\frac{2(y(LN+N_r) + N_0 Lp_{II}\gamma_b^{II})^2}{N_0^2(4Lp_{II}\gamma_b^{II} + R(LN+N_r))}\right)\right) dy, \quad (45)$$

TABLE 3. DBR and E_{sav} Comparison with the number of Subcarriers M+1, $v = log_2(M)$, L = 2^{v-p_s}, the number of permutation index-bits p_p, $N = 2^{(p_s+p_t)} - 1$, and $p_t = p_r$ for the JSTRIM-DCSK system.

Modulation	*DBR*	*E_{sav}%*
CI-DCSK1 [27]	$(v+1)/2$	
CI-DCSK2	$(v+2^v-1)(2^v-1)/2^v$	
2CI-DCSK [29]	$4(v+1)/3$	
GSIM-DCSK-I [44]	$L^2(p_s+1)/(L+1)$	$(1-1/(p_s+1))E_b$
GSIM-DCSK-II	$L^2(p_s+2^{p_s}-1)(2^{p_s}-1)/(L(2^{p_s}-1)+1)$	$(1-(2^{p_s}-1)/(ps+2^{p_s}-1))E_b$
CTIM [47]		$(1-((2^{p_s}-1)(2^{p_t}-1))/(p_s+p_t+(2^{p_s}-1)(2^{p_t}-1)))E_b$
GSPIM-DCSK-I [48]	$L^2(p_s+p_p+1)/(L+1)$	$(1-1/(p_s+p_p+1))E_b$
GSPIM-DCSK-II	$L^2(p_s+(2^{p_s}-1)(p_p+1))(2^{p_s}-1)/(L(2^{p_s}-1)+1)$	$(1-(2^{p_s}-1)/(p_s+(2^{p_s}-1)(p_p+1)))E_b$
JSTRIM-DCSK-I	$L^2(p_s+p_t+p_r+1)/(L+2^{p_r})$	$(1-1/(p_s+p_t+p_r+1))E_b$
JSTRIM-DCSK-II	$L^2N(p_s+p_t+(p_r+1)N)/(LN+2^{p_r})$	$(1-N/(p_s+p_t+(p_r+1)N))E_b$

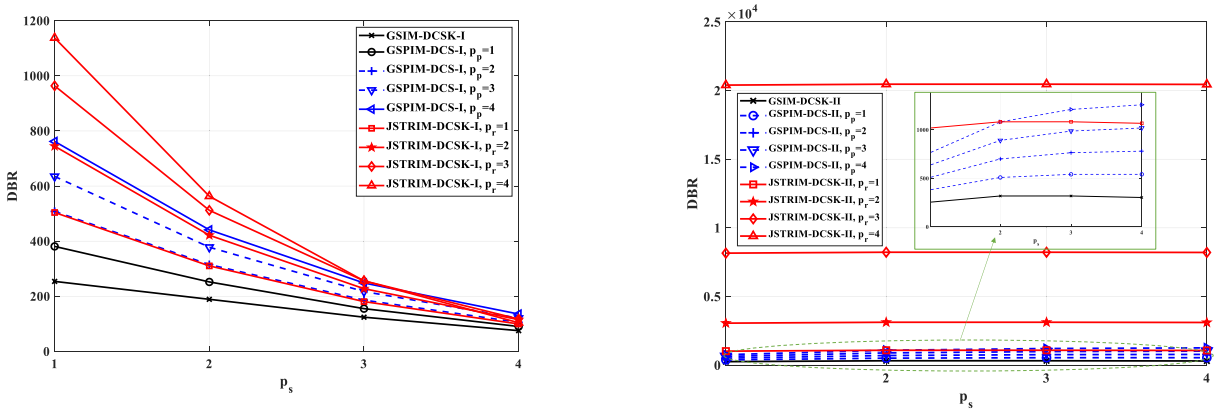

FIGURE 3. DBR comparison versus p_s for scheme I on the left and scheme II on the right. The number of subcarriers is set to $M = 256$ ($v = 8$) for all multicarrier systems. $p_r = p_t = \{1, 2, 3, 4\}$ and $p_p = \{1, 2, 3, 4\}$.

TABLE 4. Spectral efficiency comparison for different index modulation DCSK schemes with the number of permutations index bits p_p, $N = N_sN_t - 1 = (2^{(p_s+p_t)}-1)$, and $p_t = p_r$ for JSTRIM-DCSK.

Modulation	*Spectral Efficiency*
CI-DCSK1 [36]	$(v+1)/((M+1)RT_cB)$
CI-DCSK2 [36]	$(M+v-1)/((M+1)RT_cB)$
2CI-DCSK [38]	$2(v+1)/((M+1)RT_cB)$
GSIM-DCSK-I [44]	$M(p_s+1)/(2^{p_s}(M+1)RT_cB)$
GSIM-DCSK-II [44]	$M(p_s+2^{p_s}-1)/(2^{p_s}(M+1)RT_cB)$
CTIM-DCSK [47]	$(p_s+p_t+(N_s-1)(N_t-1))/((N_t+1)MRT_cB)$
GSPIM-DCSK-I [48]	$M(p_s+p_p+1)/(2^{p_s}(1+2^{p_s})RT_cB)$
GSPIM-DCSK-II [48]	$M((2^{p_s}-1)(p_p+1)+p_s)/(2^{p_s}(1+2^{p_s})RT_cB)$
JSTRIM-DCSK-I	$M(p_s+p_t+p_r+1)/(N_sN_t(M+1)RT_cB)$
JSTRIM-DCSK-II	$M(p_s+p_t+(p_r+1)N)/(N_sN_t(M+1)RT_cB)$

Table 4 presents SE comparisons for several DCSK schemes. The SE values of GRSIM-DCSK-I and GRSIM-DCSK-II were expressed in terms of the M, p, and q values.

Fig. 5 shows an SE comparison between JSTRIM-DCSK and GSIM-DCSK versus p_s, with $p_r = p_t = \{1, 2, 3, 4\}$. The SE of JSTRIM-DCSK-I decreases with increasing p_t values, consistently remaining lower than that of the GSIM-DCSK-I across all p_t and p_s values. Conversely, JSTRIM-DCSK-II exhibits an enhanced SE with increases in p_s or p_t, surpassing both the JSTRIM-DCSK-I and GSIM-DCSK systems. In Fig. 6, an SE comparison between JSTRIM-DCSK-II and GSPIM-DCSK-II is shown for $p_r = p_t = \{2, 3, 4\}$ and $p_p = \{2, 3, 4\}$. If both systems have the same duration time βT_c, it is evident that increasing p_s or p_t enhances the SE of JSTRIM-DCSK-II. Additionally, JSTRIM-DCSK-II outperformed the GSPIM-DCSK-II system in terms of the SE.

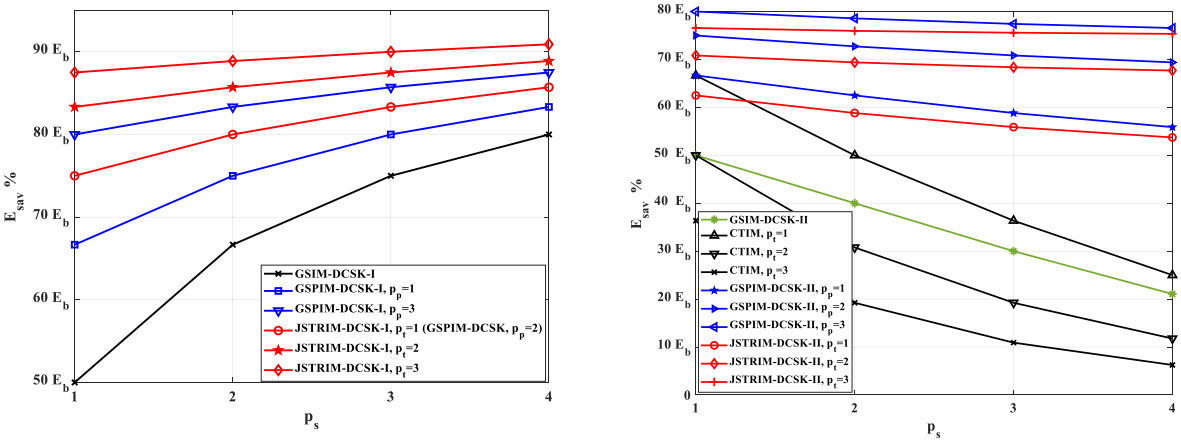

FIGURE 4. Comparison of E_{sav} percentage factors among various DCSK modulations for scheme I (left) and II (right). Comparisons are based on $p_t = 1, 2, 3$ for JSTRIM-DCSK and CTIM-DCSK, and $p_p = 1, 2, 3$ for GSPIM-DCSK.

TABLE 5. Complexity of index modulation DCSK systems at the transmitter.

Element	*CI [36]*	*2CI [38]*	*GSIM [44]*	*GSPIM [48]*	*JSTRIM*
Adder	1	2^v+1	1	1	1
Multipliers	$2^{(v+1)}+1$	3.2^v+1	$2^{(v+1)}+1$	$2^{(v+1)}+1$	$2^{(v+1)}+1$
Index Mappers/Selector	1	2	L	2L	3L
Polarity converter	2	1	L	L	L
PSF	1	2	1	1	2^v+1
Hilbert filter	0	1	0	0	0
Additional Block	0	0	0	Permutation Block	Gram-Schmidt+ Concatenation

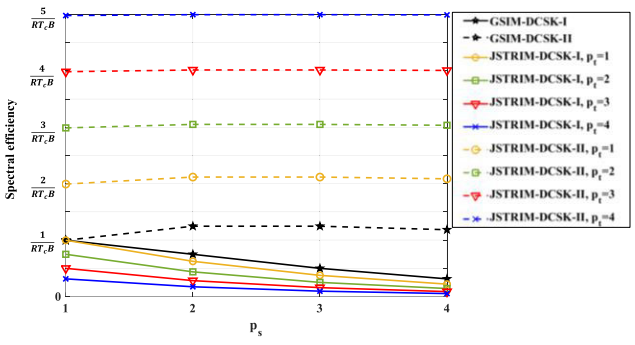

FIGURE 5. Spectral efficiency of GSIM-DCSK and JSTRIM-DCSK systems with $M = 256$ subcarriers for all multicarrier systems and $p_r = p_t = \{1, 2, 3, 4\}$.

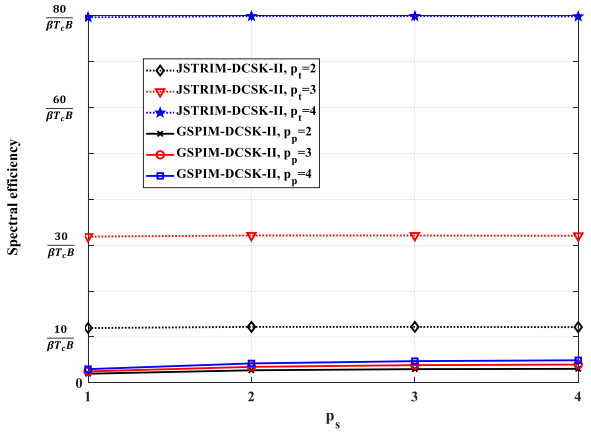

FIGURE 6. Comparison of spectral efficiency between GSPIM-DCSK and JSTRIM-DCSK systems versus p_s. The number of subcarriers is set to $M = 256$ ($v = 8$) for all multicarrier systems. $p_r = p_t = \{2, 3, 4\}$, $p_p = \{2, 3, 4\}$.

C. COMPLEXITY ANALYSIS

The hardware complexity of the JSTRIM-DCSK system is compared with that of the GSPIM-DCSK, GSIM-DCSK, carrier index DCSK (CI-DCSK), and two-layer carrier index modulation (2CI-DCSK) systems on the sending and reception sides in Tables 5 and 6. All systems are assumed to have approximately the same number of subcarriers, $M = 2^v$ with the total number of transmitted bits specified. The operational complexity (OC) factor from [44] is employed to compare the system complexity, defined as the number of multiplications processed in the spreading/despreading component per total transmitted bits over the duration of βT_c. The focus is on the multiplications involved in modulating bits with a chaotic sequence at the transmitter as well as those required at the receiver during energy detection, where the reference chaotic sequence is multiplied by the information-bearing sequence.

TABLE 6. Complexity index modulation DCSK systems at the receiver.

Element	*CI [36]*	*2CI [38]*	*GSIM [44]*	*GSPIM [48]*	*JSTRIM*
Multipliers	2^v+1	2^v+1	2^v+1	2^v+1	2^v+1
Matched filter	2^v+1	2^v+1	2^v+1	2^v+1	2^v+1
Energy detector	2^v	2^{v+1}	2^v	2^{v+p_p}	$2^{v+p_r+p_t}$
Another block	0	Hilbert filter	0	Permutation generator	Framing

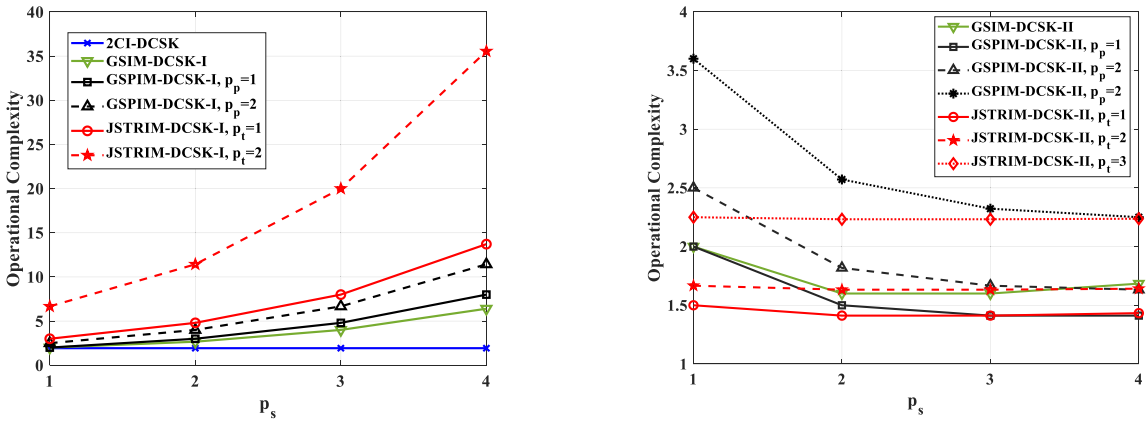

FIGURE 7. OC factor of index modulation DCSK systems, with schemes I on the left and schemes II on the right. The value of OC is normalized by R and $p_t = p_r = 1, 2, 3$ for JSTRIM-DCSK and $p_p = 1, 2, 3$ for GSPIM-DCSK.

TABLE 7. The operational complexity (OC) factor of several index modulation DCSK schemes.

Modulation	*Operational Complexity (OC)*
MC-DCSK [25]	$(2^vR+2^vR)/2^v = 2R$
CI-DCSK1 [36]	$(2^vR+2^vR)/(v+1) = 2^{v+1}R/(v+1)$
CI-DCSK2 [36]	$(2^vR+2^vR)/(2^v+v-1) = 2^{v+1}R/(2^v+v-1)$
2CI-DCSK [38]	$(2^{v+1}R+2^{v+1}R)/(2(v+1)) = 2^{v+1}R/(v+1)$
GSIM-DCSK-I [44]	$(2^vR+2^vR)/(2^{(v-p_s)}\,(p_s+1)) = 2^{p_s+1}R/(p_s+1)$
GSIM-DCSK-II [44]	$(2^vR+2^vR)/(2^{(v-p_s)}\,(2^{p_s}+p_s-1)) = 2^{p_s+1}R/\,(2^{p_s}+p_s-1)$
GSPIM-DCSK-I [48]	$(2^vR+2^{v+p_p}R)/(2^{(v-p_s)}\,(p_s+p_p+1)) = 2^{p_s}(1+2^{p_p})R/(p_s+p_p+1)$
GSPIM-DCSK-II [48]	$\dfrac{(2^vR+2^{v+p_p}R)}{2^{(v-p_s)}\,(p_s+(p_p+1)(2^{p_s}-1))} = \dfrac{2^{p_s}(1+2^{p_p})R}{(p_s+(p_p+1)(2^{p_s}-1))}$
JSTRIM-DCSK-I	$\dfrac{(2^{v+p_t}\,R+2^v2^{p_t+p_r}R)}{2^{(v-p_s)}\,(p_s+p_t+p_r+1)} = \dfrac{2^{p_s+p_t}(1+2^{p_r})R}{(p_s+p_t+p_r+1)}$
JSTRIM-DCSK-II	$\dfrac{(2^{v+p_t}\,R+2^v2^{p_t+p_r}R)}{2^{(v-p_s)}\,(p_s+p_t+(p_r+1)N)} = \dfrac{2^{p_s+p_t}(1+2^{p_r})R}{(p_s+p_t+(p_r+1)N)}$

Table 7 and Fig. 7 present the OC factors for different index modulations and proposed systems. Notably, increasing p_s or p_t resulted in an increased complexity for the two proposed systems. For the JSTRIM-DCSK-I system shown in Fig. 7a, the OC factor exceeded those of GSIM-DCSK-I, GSPIM-DCSK-I, and 2CI-DCSK across and 2CI-DCSK across all values of p_s. In the case of the JSTRIM-DCSK-II system in Fig. 8b, the OC factor of JSTRIM-DCSK-II ($p_t = 1$) is lower than that of GSIM-DCSK-II for all p_s p-values and lower than that of GSPIM-DCSK-II ($p_p = 1$) for p_s less than 3. Moreover, the OC factors of JSTRIM-DCSK-II with $p_t = 2$ and 3 are lower than those of GSPIM-DCSK-II with $p_p = 2$ and 3, respectively.

The OC increases significantly as either p_t or p_s approaches infinity. Specifically, in the JSTRIM-DCSK-I system, when either either p_t or p_s increases without bound, the OC also becomes infinity. For the JSTRIM-DCSK-II system, there are two p_s is held constant while p_t approaches infinity, the OC becomes infinity; alternatively, if p_t is held constant and p_s

approaches infinity, the OC converges to the value $\frac{2^{p_t}(1+2^{p_t})R}{((p_t+1)2^{p_t})}$.

V. SIMULATION RESULTS AND DISCUSSION

In this section, we present the analytical and simulated performance of the two proposed systems to validate the analysis and compare the results with recent index modulation techniques, including the 2CI-DCSK, CI-DCSK, GSIM-DCSK, and GSPIM-DCSK systems, under both AWGN and MRFC conditions. The MRFC is characterized by equal average power gains $E\left(\alpha_1^2\right) = E\left(\alpha_2^2\right) = E\left(\alpha_3^2\right) = \frac{1}{3}$ and time delays $\tau_1 = 0$, $\tau_2 = 2$, and $\tau_3 = 5$.

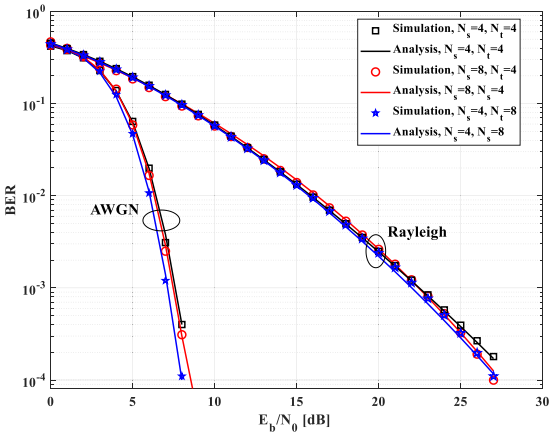

FIGURE 8. Impact of N_S and N_t on the BER performance of JSRTIM-DCSK-I for $R = 64$ and $v = 8$ ($M = 256$).

A. THEORETICAL AND SIMULATED BER PERFORMANCE

Fig. 8 illustrates the theoretical and simulated BER performances of the JSTRIM-DCSK-I scheme over AWGN and MRFC, demonstrating the impact of the number of time slots N_s and number of subcarriers N_t on the BER. The theoretical and simulated values closely match each other, confirming the accuracy of the analysis. With a fixed N_t, increasing N_s from 4 to 8 yields consistent BER performance in both AWGN and MRFC. Conversely, when N_s is fixed and N_t increased from 4 to 8, there is a slight BER improvement of approximately 1 dB at a BER of 10^{-3}. Fig. 9 depicts the theoretical and simulated BER performances JSTRIM-DCSK-II over AWGN and MRFC, showing the influence of N_s and N_t on the BER. The theoretical and simulated BER were aligned closely to verify the accuracy of the analysis.

To illustrate the impact of the subcarrier number M on the performance of the JSTRIM-DCSK-I and JSTRIM-DCSK-II systems, Fig. 10 shows the BER performance over the AWGN and MRFC channels with $R = 64$, $N_s = N_t = 4$, and $M = 64$ and 256. Increasing M enhances system performance, which is particularly evident in JSTRIM-DCSK-I.

For instance, at a BER of 10^{-3}, the JSTRIM-DCSK-I system with $M = 256$ achieves a 0.7 dB gain over that with $M = 64$ over AWGN. Moreover, with $M = 64/256$, the

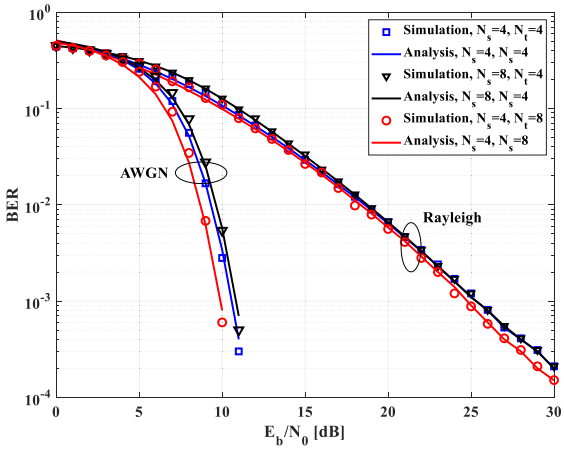

FIGURE 9. Impact of N_S and N_t on the BER performance of JSRTIM-DCSK-II for $R = 64$ and $v = 8$ ($M = 256$).

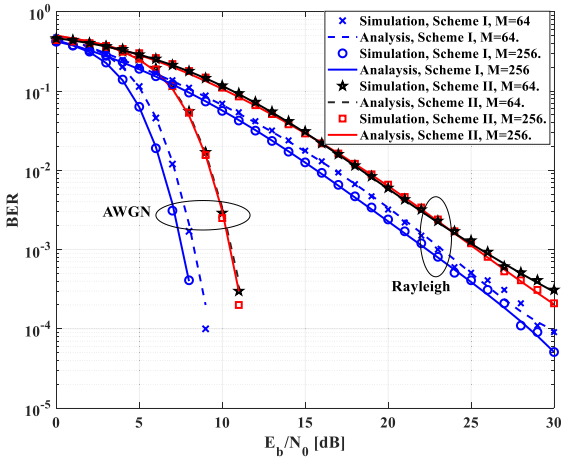

FIGURE 10. Impact of the number of subcarriers M on the BER performance of JSTRIM-DCSK scheme I and II systems for $R = 64$, $N_S = N_t = 4$, and $M = 64, 256$.

total transmitted bits are 28/112 bits and 196/784 bits for JSTRIM-DCSK-I and JSTRIM-DCSK-II, respectively. Thus, increasing v ($v = log_2 M$) from six to eight improves the total number of transmitted bits in both systems.

B. BER PERFORMANCE COMPARISON WITH OTHER SYSTEMS

Fig. 11 compares the BER performance of the proposed JSTRIM-DCSK systems with those of the GSIM-DCSK systems over AWGN and MRFC for the same number of subcarriers. Parameters are set as $M = 256, R = 64, \beta = 256, p_s = 4, p_t = p_r = 2$, and $L = 16$. The JSTRIM-DCSK-I scheme exhibits superior BER performance compared with the JSTRIM-DCSK-II and GSIM-DCSK systems over both AWGN and MRFC. For instance, in an AWGN channel, JSTRIM-DCSK-I achieves gains of approximately 5, 6, and 10 dB over GSIM-DCSK-I, JSTRIM-DCSK-II, and GSIM-DCSK-II, respectively, at a BER of 10^{-3}. In an MRF approximately 2, 3, and 7 dB over the same systems at the same BER value. In addition, JSTRIM-DCSK-II

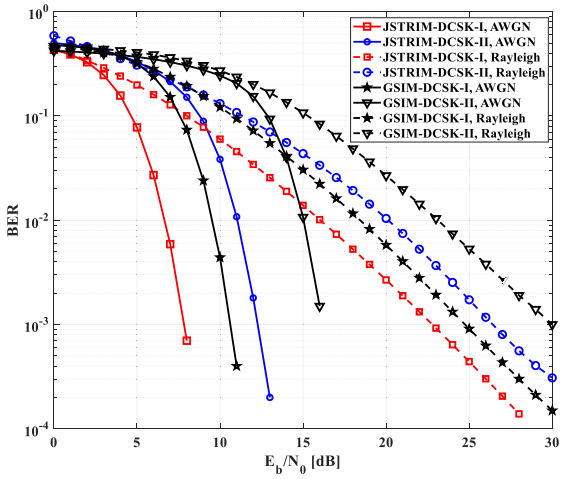

FIGURE 11. BER of JSTRIM-DCSK and GSIM-DCSK systems with $R = 64$, $\beta = 256$, $p_s = 4$, $p_t = p_r = 2$, $L = 16$, and the same number of subcarriers ($M = 256$).

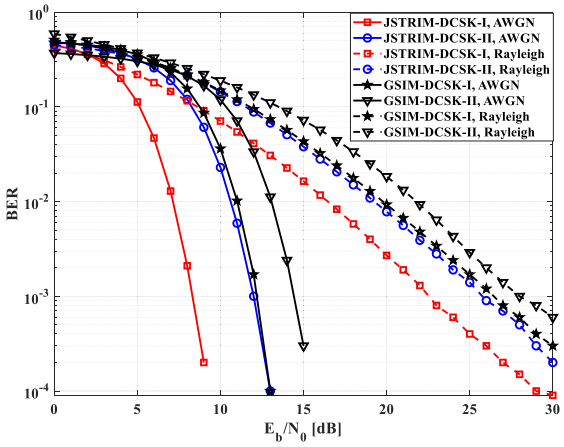

FIGURE 12. BER performance of JSTRIM-DCSK and GSIM-DCSK systems with the same number of transmitted bits.

outperformed GSIM-DCSK-II by approximately 5 and 3 dB over AWGN and MRFC, respectively.

In Fig. 12, the BER performance of the JSTRIM-DCSK system is compared with that of the GSIM-DCSK system by using approximately 100 bits. The parameters for JSTRIMDCSK-I, JSTRIM-DCSK-I, GSIM-DCSK-I, and GSIM-DCSK-II were set as ($p_s = 2$, $p_t = p_r = 2$, $v = 6$, 112 bits),($p_s = 2$, $p_t = p_r = 2$, $v = 3$, 98 bits),($p_s = 2$, $v = 7$, 96 bits), and ($p_s = 2$, $v = 6$, respectively. Despite the different information rates, efforts were made to ensure comparable rates for fair comparison. At a BER of 10^{-3} and a similar number of transmitted bits, JSTRIM-DCSK-II outperformed GSIM-DCSK-II by approximately 1 and 4 dB over AWGN and MRFC, respectively. In addition, JSTRIM-DCSK-II demonstrated a BER performance comparable to that of the GSIM-DCSK-I scheme.

In Fig. 13, the BER performances of the proposed and GSPIM-DCSK systems under AWGN and MRFC conditions using the same number of subcarriers are shown. The total number of transmitted bits is 144, 3120, 112,

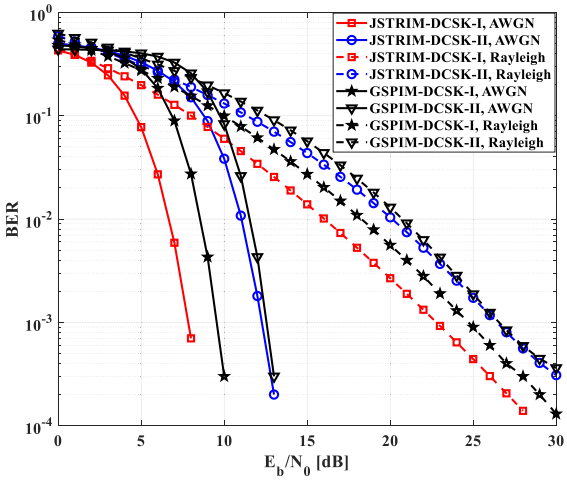

FIGURE 13. BER performance of JSTRIM-DCSK and GSPIM-DCSK systems over AWGN and MRFC with $R = 64$, $\beta = 256$, $p_s = 4$, $p_t = p_r = 2$, $L = 16$, and the same number of subcarriers ($M = 256$). The parameters setting for GSPIM-DCSK are ($p_s = 4$, $p_p = 2$, $\beta = 256$).

and 764 for JSTRIM-DCSK-I, JSTRIM-DCSK-II, GSPIM-DCSK-I ($p_s = 4$, $p_p = 2$), and GSPIM-DCSK-II ($p_s = 4$, $p_p = 2$), respectively.

In Fig. 14, the JSTRIM-DCSK schemes are compared with GSPIM-DCSK systems using approximately 100 bits. The parameters for GSPIM-DCSK-I and GSPIM-DCSK-II were set to ($p_s = 2$, $p_p = 3, v = 6,96$ bits) and ($p_s = 2$, $p_p = 2, v = 5,88$ bits), respectively. At the same subcarrier number and BER of 10^{-3}, JSTRIM-DCSK-I outperforms other index modulations over AWGN and MRFC, with gains with gains of approximately 1, 4, and 4.5 dB compared to the GSPIMDCSK-I, JSTRIM-DCSK-II, and GSPIM-DCSK-II systems, respectively. Additionally, the JSTRIM-DCSK-II and and GSPIM-DCSK-II systems exhibit similar BER performances for both AWGN and MRFC.

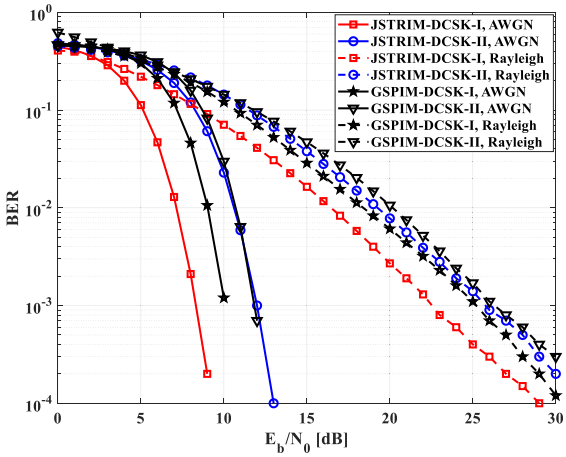

FIGURE 14. BER performance of JSTRIM-DCSK and GSPIM-DCSK systems over AWGN und MRFC with matched numbers of transmitted bits.

In Fig. 15, the BER performance of JSTRIM-DCSK schemes are compared with $p_s = 4, 5$ and $p_t = 4, 5$,

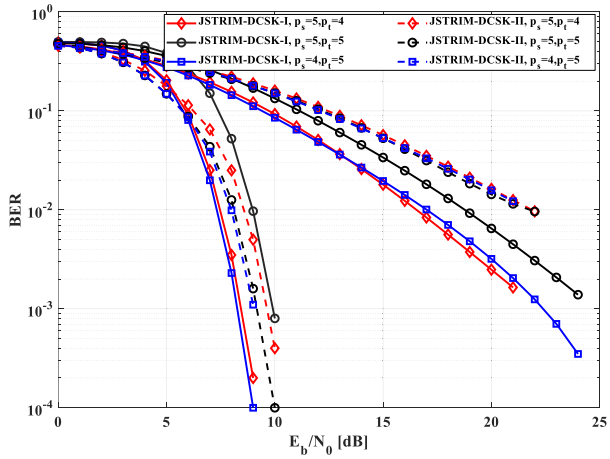

FIGURE 15. BER performance of JSTRIM-DCSK systems with $R = 64$, $\beta = 2024$, $p_s = 4,5$, $p_t = p_r = 4,5$, $L = 16,32$ and the same number of subcarriers ($M = 512$). The solid lines refer to the JSTRIM-DCSK-I and the dashed lines to the JSTRIM-DCSK-II systems.

where $v = 9$. This comparison illustrates the effectiveness of the proposed schemes for significantly large values of index bits, not exceeding 5 bits. The results demonstrate that the JSTRIM-DCSK-I system outperforms the JSTRIM-DCSK-II system in two situations: over MRFC and over AWGN when $p_s = 4$, $p_t = 5$ and $p_s = 5, p_t = 4$. However, the performance of the JSTRIM-DCSK-I slightly degrades when $p_s = 5$ and $p_t = 5$ as compared to STRIM-DCSK-II. Additionally, the BER performance of JSTRIM-DCSK-II exhibits a more gradual change over MRFC, indicating its robustness under multipath fading conditions. These observations provide valuable insights into the optimal configuration of the proposed schemes under different channel conditions and index bit allocations.

VI. CONCLUSION

In this study, we propose the Joint Subcarrier Time Reference Index Modulation assisted DCSK (JSTRIM-DCSK) system, which leverages subcarrier index, time slot index, and reference index modulation for efficient data transmission. Two variants, JSTRIM-DCSK-I and JSTRIM-DCSK-II, are presented to optimize the resource allocation for enhanced performance. A comprehensive comparative analysis of demonstrates the superior energy and spectral efficiency of JSTRIM-DCSK while maintaining manageable complexity. Analytical BER derivation and simulation results confirm its effectiveness and show improved performance over current systems. While it is in principle possible to extend to higher-order modulation schemes to increase bit capacity, this may negatively impact BER performance, increase bit interference, and increase system complexity. Therefore, future research will investigate these higher order schemes, as well as schemes using all subcarriers and time slots, and their comparative performance to evaluate the tradeoffs. In the meantime, JSTRIM-DCSK is a promising candidate for high data rate applications in DCSK index modulation.

REFERENCES

[1] G. Kolumbán, G. K. Vizvári, W. Schwarz, and A. Abel, "Differential chaos shift keying: A robust coding for chaotic communication," in *Proc. Int. Workshop Nonlinear Dynam. Electron. Syst.*, Seville, Spain, 1996, pp. 92–97.

[2] G. Kaddoum, "Wireless chaos-based communication systems: A comprehensive survey," *IEEE Access*, vol. 4, pp. 2621–2648, 2016.

[3] Y. Fang, G. Han, P. Chen, F. C. M. Lau, G. Chen, and L. Wang, "A survey on DCSK-based communication systems and their application to UWB scenarios," *IEEE Commun. Surveys Tuts.*, vol. 18, no. 3, pp. 1804–1837, 3rd Quart., 2016.

[4] Y. Fang, J. Xu, L. Wang, and G. Chen, "Performance of MIMO relay DCSK-CD systems over Nakagami fading channels," *IEEE Trans. Circuits Syst. I, Reg. Papers*, vol. 60, no. 3, pp. 757–767, Mar. 2013.

[5] C. Bai, H.-P. Ren, and J. Li, "A differential chaos-shift keying scheme based on hybrid system for underwater acoustic communication," in *Proc. IEEE/OES China Ocean Acoust. (COA)*, Jan. 2016, pp. 1–5.

[6] G. Kaddoum and N. Tadayon, "Differential chaos shift keying: A robust modulation scheme for power-line communications," *IEEE Trans. Circuits Syst. II, Exp. Briefs*, vol. 64, no. 1, pp. 31–35, Jan. 2017.

[7] F. S. Hasan, "Design and analysis of three-way relay network coding schemes based differential chaos shift keying communication system," *Wireless Pers. Commun.*, vol. 114, no. 1, pp. 29–47, Sep. 2020.

[8] P. Mukherjee, C. Psomas, and I. Krikidis, "Differential chaos shift keying-based wireless power transfer," in *Proc. IEEE Int. Conf. Acoust., Speech Signal Process. (ICASSP)*, Jun. 2021, pp. 4895–4899.

[9] G. Narang, M. Aggarwal, H. Kaushal, A. Kumar, and S. Ahuja, "Performance analysis of differential chaos shift keying in free space optical communication with diversity techniques," *IEEE Access*, vol. 11, pp. 54438–54447, 2023.

[10] Z. Galias and G. M. Maggio, "Quadrature chaos-shift keying: Theory and performance analysis," *IEEE Trans. Circuits Syst. I, Fundam. Theory Appl.*, vol. 48, no. 12, pp. 1510–1519, Dec. 2001.

[11] H. Yang and G.-P. Jiang, "High-efficiency differential-chaos-shift-keying scheme for chaos-based noncoherent communication," *IEEE Trans. Circuits Syst. II, Exp. Briefs*, vol. 59, no. 5, pp. 312–316, May 2012.

[12] W. K. Xu, L. Wang, and G. Kolumbán, "A new data rate adaption communications scheme for code-shifted differential chaos shift keying modulation," *Int. J. Bifurcation Chaos*, vol. 22, no. 8, Aug. 2012, Art. no. 1250201.

[13] W. Xu, L. Wang, and C.-Y. Chi, "A simplified GCS-DCSK modulation and its performance optimization," *Int. J. Bifurcation Chaos*, vol. 26, no. 13, Dec. 2016, Art. no. 1650213.

[14] G. Kaddoum and F. Gagnon, "Design of a high-data-rate differential chaos-shift keying system," *IEEE Trans. Circuits Syst. II, Exp. Briefs*, vol. 59, no. 7, pp. 448–452, Jul. 2012.

[15] L. Wang, G. Cai, and G. R. Chen, "Design and performance analysis of a new multiresolution M-ary differential chaos shift keying communication system," *IEEE Trans. Wireless Commun.*, vol. 14, no. 9, pp. 5197–5208, Sep. 2015.

[16] G. Cai, Y. Fang, and G. Han, "Design of an adaptive multiresolution M-ary DCSK system," *IEEE Commun. Lett.*, vol. 21, no. 1, pp. 60–63, Jan. 2017.

[17] G. Cai, Y. Fang, G. Han, F. C. M. Lau, and L. Wang, "A square-constellation-based M-ary DCSK communication system," *IEEE Access*, vol. 4, pp. 6295–6303, 2016.

[18] G. Kaddoum, E. Soujeri, and Y. Nijsure, "Design of a short reference non-coherent chaos-based communication systems," *IEEE Trans. Commun.*, vol. 64, no. 2, pp. 680–689, Feb. 2016.

[19] T. J. Wren and T. C. Yang, "Orthogonal chaotic vector shift keying in digital communications," *IET Commun.*, vol. 4, no. 6, p. 739, 2010.

[20] S. Venkatesh and P. Singh, "An improved multiple access chaotic communication system using orthogonal chaotic vectors," in *Proc. Int. Conf. Commun. Signal Process.*, Feb. 2011, pp. 80–82.

[21] H. Yang, W. K. S. Tang, G. Chen, and G.-P. Jiang, "System design and performance analysis of orthogonal multi-level differential chaos shift keying modulation scheme," *IEEE Trans. Circuits Syst. I, Reg. Papers*, vol. 63, no. 1, pp. 146–156, Jan. 2016.

[22] G. Kaddoum and E. Soujeri, "NR-DCSK: A noise reduction differential chaos shift keying system," *IEEE Trans. Circuits Syst. II, Exp. Briefs*, vol. 63, no. 7, pp. 648–652, Jul. 2016.

[23] P. Chen, L. Shi, Y. Fang, G. Cai, L. Wang, and G. Chen, "A coded DCSK modulation system over Rayleigh fading channels," *IEEE Trans. Commun.*, vol. 66, no. 9, pp. 3930–3942, Sep. 2018.

[24] Y. Li, L. Dai, and L. Lv, "Design of an improved M-ary DCSK-aided protograph-coded communication system," *IEEE Access*, vol. 11, pp. 55002–55010, 2023.
[25] G. Kaddoum, F.-D. Richardson, and F. Gagnon, "Design and analysis of a multi-carrier differential chaos shift keying communication system," *IEEE Trans. Commun.*, vol. 61, no. 8, pp. 3281–3291, Aug. 2013.
[26] S. Li, Y. Zhao, and Z. Wu, "Design and analysis of an OFDM-based differential chaos shift keying communication system," *J. Commun.*, vol. 10, no. 3, pp. 199–205, 2015.
[27] F. S. Hasan, "Design and analysis of an OFDM-based short reference quadrature chaos shift keying communication system," *Wireless Pers. Commun.*, vol. 96, no. 2, pp. 2205–2222, Sep. 2017.
[28] F. S. Hasan and A. A. Valenzuela, "Design and analysis of an OFDM-based orthogonal chaotic vector shift keying communication system," *IEEE Access*, vol. 6, pp. 46322–46333, 2018.
[29] F. S. Hasan, M. J. Zaiter, and R. A. Mohammed, "Design and analysis of a wavelet packet modulation based differential chaos shift keying communication system," *Wireless Pers. Commun.*, vol. 109, no. 4, pp. 2439–2450, Dec. 2019.
[30] E. Basar, M. Wen, R. Mesleh, M. Di Renzo, Y. Xiao, and H. Haas, "Index modulation techniques for next-generation wireless networks," *IEEE Access*, vol. 5, pp. 16693–16746, 2017.
[31] M. Au, G. Kaddoum, M. S. Alam, E. Basar, and F. Gagnon, "Joint code-frequency index modulation for IoT and multi-user communications," *IEEE J. Sel. Topics Signal Process.*, vol. 13, no. 6, pp. 1223–1236, Oct. 2019.
[32] W. Xu and L. Wang, "CIM-DCSK: A differential chaos shift keying scheme with code-index modulation," in *Proc. 16th Int. Symp. Commun. Inf. Technol. (ISCIT)*, Qingdao, China, Sep. 2016, pp. 100–104.
[33] W. Xu, Y. Tan, F. C. M. Lau, and G. Kolumbán, "Design and optimization of differential chaos shift keying scheme with code index modulation," *IEEE Trans. Commun.*, vol. 66, no. 5, pp. 1970–1980, May 2018.
[34] W. Xu, T. Huang, and L. Wang, "Code-shifted differential chaos shift keying with code index modulation for high data rate transmission," *IEEE Trans. Commun.*, vol. 65, no. 10, pp. 4285–4294, Oct. 2017.
[35] Y. Tan, W. Xu, T. Huang, and L. Wang, "A multilevel code shifted differential chaos shift keying scheme with code index modulation," *IEEE Trans. Circuits Syst. II, Exp. Briefs*, vol. 65, no. 11, pp. 1743–1747, Nov. 2018.
[36] G. Cheng, L. Wang, W. Xu, and G. Chen, "Carrier index differential chaos shift keying modulation," *IEEE Trans. Circuits Syst. II, Exp. Briefs*, vol. 64, no. 8, pp. 907–911, Aug. 2017.
[37] G. Cheng, L. Wang, Q. Chen, and G. Chen, "Design and performance analysis of generalised carrier index M-ary differential chaos shift keying modulation," *IET Commun.*, vol. 12, no. 11, pp. 1324–1331, Jul. 2018.
[38] W. Dai, H. Yang, Y. Song, and G. Jiang, "Two-layer carrier index modulation scheme based on differential chaos shift keying," *IEEE Access*, vol. 6, pp. 56433–56444, 2018.
[39] M. Herceg, D. Vranjes, G. Kaddoum, and E. Soujeri, "Commutation code index DCSK modulation technique for high-data-rate communication systems," *IEEE Trans. Circuits Syst. II, Exp. Briefs*, vol. 65, no. 12, pp. 1954–1958, Dec. 2018.
[40] M. Herceg, G. Kaddoum, D. Vranješ, and E. Soujeri, "Permutation index DCSK modulation technique for secure multiuser high-data-rate communication systems," *IEEE Trans. Veh. Technol.*, vol. 67, no. 4, pp. 2997–3011, Apr. 2018.
[41] X. Cai, W. Xu, L. Wang, and F. Xu, "Design and performance analysis of differential chaos shift keying system with dual-index modulation," *IEEE Access*, vol. 7, pp. 26867–26880, 2019.
[42] X. Cai, W. Xu, L. Wang, and G. Kolumbán, "Multicarrier M-ary orthogonal chaotic vector shift keying with index modulation for high data rate transmission," *IEEE Trans. Commun.*, vol. 68, no. 2, pp. 974–986, Feb. 2020.
[43] X. Cai, W. Xu, F. C. M. Lau, and L. Wang, "Joint carrier-code index modulation aided M-ary differential chaos shift keying system," *IEEE Trans. Veh. Technol.*, vol. 69, no. 12, pp. 15486–15499, Dec. 2020.
[44] F. S. Hasan, "Design and analysis of grouping subcarrier index modulation for differential chaos shift keying communication system," *Phys. Commun.*, vol. 47, Aug. 2021, Art. no. 101325.
[45] X. Cai, W. Xu, L. Wang, and G. Chen, "Towards high-data-rate noncoherent chaotic communication: A multiple-mode differential chaos shift keying system," *IEEE Trans. Wireless Commun.*, vol. 20, no. 8, pp. 4888–4901, Aug. 2021.
[46] H. Ma, Y. Fang, P. Chen, S. Mumtaz, and Y. Li, "A novel differential chaos shift keying scheme with multidimensional index modulation," *IEEE Trans. Wireless Commun.*, vol. 22, no. 1, pp. 237–256, Jan. 2023.
[47] Y. Fang, J. Zhuo, H. Ma, S. Mumtaz, and Y. Li, "Design and analysis of a new index-modulation-aided DCSK system with frequency-and-time resources," *IEEE Trans. Veh. Technol.*, vol. 72, no. 6, pp. 7411–7425, Jun. 2023.
[48] B. Nazar and F. S. Hasan, "Joint grouping subcarrier and permutation index modulations based differential chaos shift keying system," *Phys. Commun.*, vol. 61, Dec. 2023, Art. no. 102213.
[49] Y. Fang, D. Peng, H. Ma, G. Han, and Y. Li, "A neural network-aided detection scheme for index-modulation DCSK system," *IEEE Trans. Veh. Technol.*, vol. 73, no. 2, pp. 2109–2121, Feb. 2024.
[50] G. Zhang, X. Wu, Y. Yang, and S. Shao, "Design and analysis of high data rate four-dimensional index modulation for differential chaos shift keying system," *IEEE Trans. Wireless Commun.*, vol. 23, no. 9, pp. 12455–12468, Sep. 2024.
[51] M. Tsagris, C. Beneki, and H. Hassani, "On the folded normal distribution," *Mathematics*, vol. 2, no. 1, pp. 12–28, Feb. 2014.

FADHIL S. HASAN was born in Baghdad, Iraq, in 1978. He received the B.Sc. degree in electrical engineering and the M.Sc. degree in electronics and communication engineering from Mustansiriyah University, Baghdad, in 2000 and 2003, respectively, and the Ph.D. degree in electronics and communication engineering from Basrah University, Iraq, in 2013.

In 2005, he joined the Faculty of Engineering, Mustansiriyah University. Since 2022, he has been a Professor with Mustansiriyah University. His recent research interests include wireless communication systems, multicarrier systems, wavelet based OFDM, MIMO systems, speech signal processing, chaotic modulation, and FPGA based communication systems.

ALEJANDRO A. VALENZUELA was born in San Carlos de Bariloche, Argentina, in 1963. He received the Dipl.-Ing. and Dr.-Ing. degrees in electrical engineering from the Technical University of Munich (TUM), Germany, in 1987 and 1992, respectively.

In 1988, he joined the Research Institute of Siemens AG in Munich, where he worked on circuit measurements and diagnostics, the development of contactless electro-optical measurement methods, and the application of high-temperature superconducting thin films. From 1992 to 1993, he contributed to the development of broadband switching systems. From 1994 to 2001, he was the Head of Development of "Broadband Peripheral Subsystems" and "Line Interface Circuits Hardware" with the Information and Communication Networks and Information and Communication Mobile Organizations at Siemens AG, Munich. Since 2001, he has been a Full Professor and the Head of the Communications Laboratory, Bonn-Rhein-Sieg University of Applied Sciences (H-BRS), Germany.